the staining of compounds, quenching of autofluorescence was performed as described previously. Quenched tissue sections were immersed in 100 μM of BF-227 or 0.125% thioflavin-S solution containing 50% ethanol for 10 min. Sections stained with each compound were then dipped briefly into water and rinsed in PBS for 60 min before coverslipping with Fluor Save Reagent (Calbiochem); sections were examined using an Eclipse E800 microscope (Nikon) equipped with a V-2A filter set (excitation, 380–420 nm; dichroic mirror, 430 nm; long-pass filter, 450 nm). Sections stained with thioflavin-S were dipped briefly in tap water and in 50% ethanol and then washed in PBS for 60 min before coverslipping; this was followed by fluorescent microscopy using a BV-2A filter set (excitation, 400–440 nm; dichroic mirror, 455 nm; long-pass filter, 470 nm). In addition, adjacent sections were immunostained using monoclonal antibody (mAb) against Aβ (6F/3D; Dako A/S). After pretreatment with 90% formic acid for 5 min, sections were immersed in blocking solution for 30 min and then incubated for 60 min at 37°C with 6F/3D at a dilution of 1:50. After incubation, sections were processed by the avidin–biotin method using a Pathostain ABC-POD(M) Kit (Wako) and diaminobenzidine tetrahydrochloride.

Labeling of Aβ Deposits in Transgenic Mouse Brain

Ex vivo plaque labeling with BF-227 was evaluated using PS1/APPsw double transgenic mice (n = 2) and a wild-type mouse (n = 1) (male, 32-wk old) (*15*). A BF-227 solution containing 10% polyethylenglycol 400 and 0.1 mol/L HCl was administered into the tail vein at a dose of 4 mg/kg. Mice were anesthetized using sodium pentobarbital 2 h after injection of BF-227; they were then perfused transcardially with ice-cold saline, which was followed by 4% paraformaldehyde in 0.1 M PBS, and the brains were removed. After cryoprotection in 30% sucrose/0.1 M PBS, 6-μm frozen sections were cut using an OTF cryostat and imaged with no additional staining for fluorescent microscopy using a V-2A filter set. The same sections were immunostained using mAb against Aβ (6F/3D) as described earlier.

Subjects and Patients in Clinical PET Study

Eleven normal (healthy) control subjects, including 3 young normal subjects and 8 aged-matched normal subjects, and 10 probable AD patients underwent PET measurement of ^{11}C-BF-227 distribution in the brain (Table 1). AD patients were recruited through the Tohoku University Hospital Dementia Patients Registry. The diagnosis of AD was made according to the National Institute of Neurological and Communicative Diseases and Stroke/Alzheimer's Disease and Related Disorders Association (NINCDS–ADRDA) criteria. The normal control group was recruited from volunteers, who were taking no centrally acting medication, had no cognitive impairment, and had no cerebrovascular lesion on MR images. No significant difference in age was apparent between the AD group and the aged normal control group. AD patients had significantly lower mean mini-mental status examination (MMSE) scores than normal control subjects. This study was approved by the ethics committee on clinical investigations of Tohoku University School of Medicine and was performed in accordance with the Declaration of Helsinki. After complete description of the study to the patients and subjects, written informed consent was obtained.

Image Acquisition Protocols

The protocol of the PET study was approved by the Committee on Clinical Investigation at The Tohoku University School of Medicine and the Advisory Committee on Radioactive Substances at Tohoku University. The ^{11}C-BF-227 PET study was performed using a SET-2400W PET scanner (Shimadzu). After intravenous injection of 211–366 MBq of ^{11}C-BF-227, dynamic PET images were obtained for 60 min (23 sequential scans: 5 scans × 30 s, 5 scans × 60 s, 5 scans × 150 s, and 8 scans × 300 s) with each subject's eyes closed. The T1-weighted MR images were obtained using a SIGNA 1.5-T machine (GE Healthcare).

TABLE 1
Subject Demographics

Group	Subject	Sex	Age (y)	MMSE score
Young normal (n = 3)	YN 1	M	36	30
	YN 2	M	37	30
	YN 3	M	36	30
	Mean ± SD		36.3 ± 0.6	30.0 ± 0.0
Aged normal (n = 8)	AN 1	M	69	30
	AN 2	F	70	29
	AN 3	F	64	30
	AN 4	F	65	30
	AN 5	M	67	30
	AN 6	M	69	30
	AN 7	M	71	30
	AN 8	M	59	30
	Mean ± SD		66.8 ± 4.0	29.9 ± 0.4
All normal (n = 11)	Mean ± SD		58.5 ± 14.6	29.9 ± 0.3
AD (n = 10)	AD 1	F	65	24
	AD 2	M	75	19
	AD 3	F	72	21
	AD 4	F	82	18
	AD 5	F	62	20
	AD 6	F	68	21
	AD 7	M	70	23
	AD 8	F	85	23
	AD 9	M	78	14
	AD 10	F	75	26
	Mean ± SD		73.2 ± 7.3*	20.9 ± 3.4*†

*P < 0.05 vs. young normal group.
†P < 0.05 vs. aged normal group.
MMSE = mini-mental state examination.

Image Analysis

First, standardized uptake value (SUV) images of ^{11}C-BF-227 were obtained by normalizing tissue radioactivity concentration by injected dose and body weight. Subsequently, individual MR images were anatomically coregistered into individual PET images using Statistical Parametric Mapping software (SPM2; Wellcome Department, U.K.) (*16*). Regions of interest (ROIs) were placed on individual axial MR images in the cerebellar hemisphere, striatum, thalamus, frontal cortex (Brodmann's areas [BA] 8, 9, 10, 44, 45, 46, and 47), lateral temporal cortex (BA 21, 22, 37, and 38), parietal cortex (BA 39 and 40), temporooccipital cortex (BA 18 and 19), occipital cortex (BA 17), medial temporal cortex (BA 27, 28, 34, and 35), pons, and subcortical white matter, as described previously (*17*). The ROI information was then copied onto dynamic PET SUV images, and regional SUVs were sampled using Dr.View/LINUX software (Asahi-Kasei Joho System).

The interrater reliability for the ROI measurement was tested between 2 raters in 14 subjects and patients. The intraclass correlation coefficient was 0.95 in the frontal cortex and cerebellum, 0.97 in the lateral temporal and parietal cortices, and 0.98 in the medial temporal cortex. The correlation coefficient between these 2 measurements was 0.96 in the frontal cortex, 0.97 in the lateral temporal cortex, and 0.99 in the parietal cortex, medial temporal cortex, and cerebellum. SUVs between 40 and 60 min were averaged to calculate the SUVs for group comparison.

Statistical Analysis

For statistical comparison in the 3 groups, we applied the Kruskal–Wallis test, which was followed by Dunn's multiple comparison test. The difference in time–activity curves in ^{11}C-BF-227 PET was also evaluated by repeated measures ANOVA, which was followed by the Bonferroni–Dunn post hoc test. For statistical comparisons of PET measurements in aged normal and AD groups, we used the Mann–Whitney U test. Effect-size coefficients (Cohen's d) were also calculated for the evaluation of group differences in PET measurements. Statistical significance for each analysis was defined as $P < 0.05$. Statistical comparison between images from normal control subjects and AD patients was performed on a voxel-by-voxel basis using SPM2 software (*16*). SUV summation images 30–60 min after injection were stereotactically normalized using individual MR images into a standard space of Talairach and Tournoux. The normalized images were smoothed using a $16 \times 16 \times 16$ mm gaussian filter. The count of each voxel was normalized to the cerebellar ROI value, because cerebellum is reported to be a region free of fibrillar amyloid plaques in AD brain. Images of patients with AD ($n = 10$) were compared with those of aged normal control subjects ($n = 8$) for between-group analysis ($P < 0.001$, uncorrected; extent threshold, $k = 200$). For the group analysis, a 2-sample t test was used to detect differences between the AD and normal control groups.

RESULTS

In Vitro Binding Study for Aβ Fibrils

In vitro binding assay indicated that BF-227 shows high binding affinity for Aβ1-42 fibrils. K_i for Aβ1-42 fibrils in competitive binding assay using ^{125}I-BF-180 was 4.3 ± 1.5 nM in BF-227, comparable to levels previously reported for compound BF-168.

Neuropathologic Staining in AD Brain Sections

Neuropathologic examination using BF-227 indicated that amyloid plaques were selectively stained with BF-227 in AD brain sections (Fig. 2A). Especially, cored plaques were brightly stained with BF-227, indicating that this compound preferentially binds to mature amyloid plaque. This staining pattern correlated well with Aβ immunostaining in adjacent sections (Fig. 2B, arrows). BF-227 staining was further compared with staining using thioflavin-S. In contrast to clear staining of SPs and NFTs with thioflavin-S (Fig. 2C), BF-227 primarily stained SPs, with faint staining of NFTs (Fig. 2B, arrowheads). No apparent staining was also observed in the temporal brain section of the aged normal case (Fig. 2D).

BBB Permeability and Clearance from Normal Brain

Next, we investigated whether BF-227 entered the brain in amounts sufficient for use as a PET agent. The log P value of BF-227 was 1.75, close to that of BF-168 (log P = 1.79). Intravenous administration of BF-227 into normal mice indicated that this compound readily penetrated the BBB. Brain uptakes at 2, 10, 30, and 60 min after intravenous injection of ^{11}C-BF-227 were 7.9 ± 1.3, 3.7 ± 0.37, 1.4 ± 0.36, and 0.64 ± 0.15 %ID/g, respectively. ^{11}C-BF-227 displayed double the initial uptake and faster washout

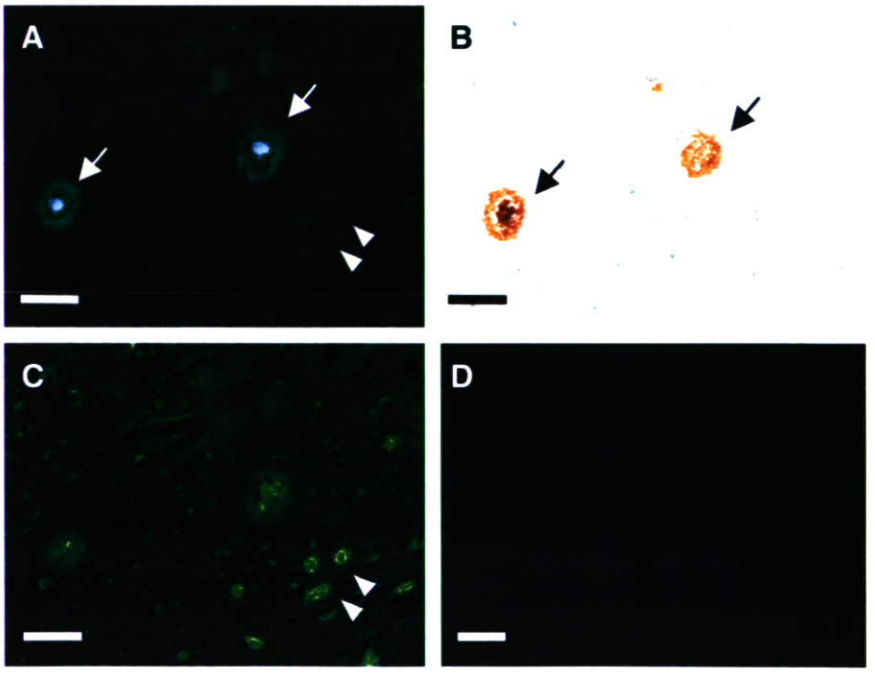

FIGURE 2. Neuropathologic staining of human brain sections by BF-227. Amyloid plaques are clearly stained with BF-227 in AD temporal brain sections (A). BF-227 staining correlates well with Aβ immunostaining in adjacent sections (B, arrows). BF-227 faintly stains NFTs, in contrast to clear staining with thioflavin-S (C, arrowheads). In aged normal temporal cortex (D), no staining by BF-227 is observed. Bar in A–C = 50 μm; bar in D = 200 μm.

in normal brain tissue compared with those of ^{18}F-BF-168 (3.9 %ID/g at 2 min after injection; 1.3 %ID/g at 60 min after injection).

Intravenous Administration of BF-227 in Transgenic Mice

In vivo binding of nonlabeled BF-227 to Aβ deposits was examined using PS1/APPsw double transgenic mice. After intravenous injection of 4 mg/kg BF-227, ex vivo observation of transgenic mouse brain slices showed numerous fluorescent spots in the neocortex and hippocampus (Figs. 3A and 3B). In contrast, no fluorescent spots were detected in the wild-type mouse brain (Fig. 3C). Brain sections of transgenic mice were subsequently immunostained using Aβ-specific antibody, and the distribution of plaques labeled with BF-227 corresponded well with Aβ immunostaining (Fig. 3D, arrowheads).

Time–Activity Data of ^{11}C-BF-227 in Clinical PET Study

No toxic event was observed in the current clinical trial of ^{11}C-BF-227. The SUV time–activity curves from ^{11}C-BF-227 PET in AD patients and all normal subjects are shown in Figure 4. Both groups showed rapid entry of ^{11}C-BF-227 into gray matter areas. In AD patients, the frontal, temporal, and parietal cortices, areas known to contain high concentrations of fibrillar amyloid plaques in AD, retained ^{11}C-BF-227 to a greater extent during the later time points compared with normal subjects (Figs. 4A–4C). When the 2 groups were compared, a significant difference in time–activity curves was observed in the frontal (Fig. 4A), lateral temporal (Fig. 4B), parietal (Fig. 4C), and visual association cortices (data not shown). In contrast, time–activity curves in the cerebellum (Fig. 4D), an area lacking fibrillar amyloid plaques, were nearly identical in normal subjects and AD patients. The subcortical white matter region showed relatively lower entry and slower clearance than gray matter areas but no significant difference in time–activity curves between the 2 groups (data not shown). In the comparison of time–activity curves in the cortical areas and cerebellum, AD patients showed a significant difference in time–activity curves over 10 min after administration of ^{11}C-BF-227, but normal subjects showed no significant differences.

SUV Images in AD Patients and Normal Control Subjects

SUV images summed over 20−40 min after injection of an aged normal subject (70-y-old woman) and an AD patient (68-y-old woman; MMSE score = 21) are shown in Figure 5. Cortical retention of ^{11}C-BF-227, especially in the basal portion of the frontal, temporal, and parietal region, was evident in the AD patient, in contrast with the images of the aged normal subject. This pattern of distribution is consistent with the findings of neuritic plaque distribution in postmortem AD brains (*18*). Higher retention of ^{11}C-BF-227 was also observed in the brainstem and thalamus; however, similar retention in these areas was detected in the aged normal subject. ^{11}C-BF-227 uptake in the cerebellum was relatively sparse in both the aged normal subject and the AD patient.

Comparisons of Regional SUVs and SUV Ratios

In the quantitative comparison of regional SUVs between 40 and 60 min after administration, cortical regions showed the tendency to be increased in AD patients; however, the difference was not significant because of the large individual difference in SUVs. SUVs in the thalamus, pons, and white matter were similar in the 3 groups. Because there were no plaques in the cerebellum, there was no BF-227 binding and no significant difference in the SUV between AD and normal groups, indicating that the cerebellum is adequate as a reference region. Therefore, the ratio of regional SUV to cerebellar SUV (SUV ratio) was calculated as an index of ^{11}C-BF-227 retention. This analysis successfully reduced the intersubject variability, as reflected in low SD values (Table 2). The mean SUV ratio for the frontal, lateral temporal, parietal, temporooccipital, occipital, anterior and posterior cingulate cortices, and striatum was significantly greater in AD patients than that in aged normal subjects (Table 2; Fig. 6). Notably, the SUV ratio in the lateral temporal cortex showed no overlap between AD patients and normal control subjects (Fig. 6). The SUV ratio in the medial temporal cortex, thalamus,

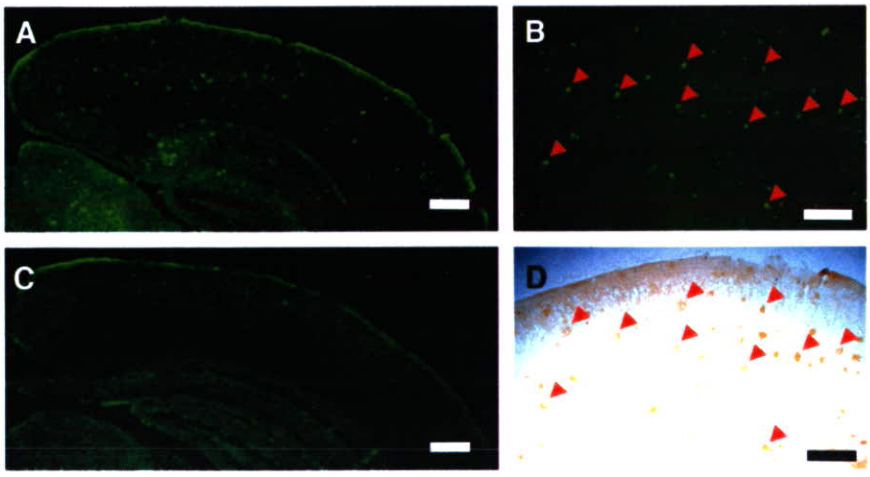

FIGURE 3. In vivo binding of BF-227 to amyloid plaques in PS1/APP transgenic mouse. In brain sections from PS1/APP transgenic mouse after intravenous injection of 4 mg/kg BF-227, numerous fluorescent spots were observed in neocortex and hippocampus of brain (A and B). In contrast, no fluorescent spots were observed in brain of wild-type mouse (C). Distribution of plaques labeled with BF-227 corresponded well with Aβ immunostaining in same section (B and D, arrowheads).

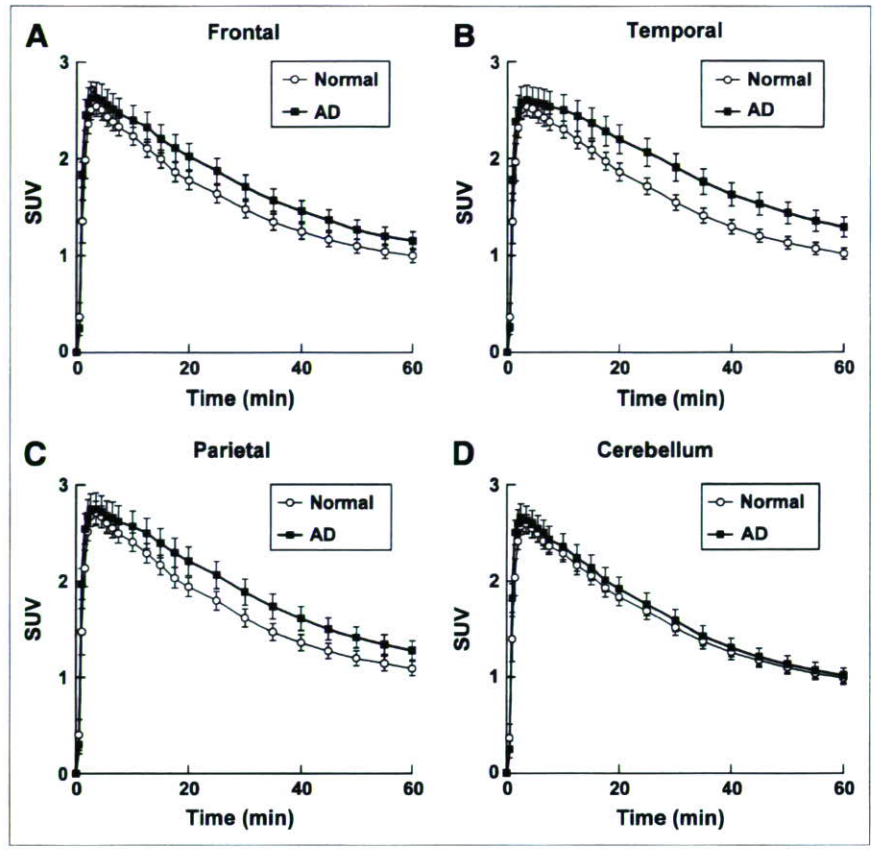

FIGURE 4. Time–activity data for ^{11}C-BF-227 PET in humans. SUV time–activity curves of ^{11}C-BF-227 in frontal cortex (A), temporal cortex (B), parietal cortex (C), and cerebellum (D) are shown. Each point represents mean ± SEM of data from 7 AD patients and 7 normal control subjects.

pons, and white matter was nearly identical in AD patients and normal subjects. The effect size between AD patients and aged normal subjects was highest in the lateral temporal cortex, which was followed by the parietal, anterior cingulate, and frontal cortices, and was lowest in the medial temporal, thalamus, and pons (Table 2). No significant difference was observed in any brain regions between young normal and aged normal subjects, although aged individuals tended to exhibit a higher SUV ratio in the frontal cortex than young individuals (data not shown).

Voxel-by-Voxel Analysis of ^{11}C-BF-227 PET Images

In comparison with aged normal subjects, AD patients showed significantly higher uptake of ^{11}C-BF-227 in the bilateral temporoparietal region ([50, −56, 6], Z = 5.41, k = 22,823), including the posterior cingulate cortex and the left middle frontal gyrus ([−26, 24, 40], Z = 3.79, k = 1,401) in SPM analysis (Fig. 7). These areas corresponded well with the region containing a high density of neuritic plaques. In contrast, no significant region was detected showing lower uptake of ^{11}C-BF-227 in the AD group than that in the normal group.

DISCUSSION

BF-227 was designed to improve BBB penetration and clearance from normal brain tissue, without deteriorating the high binding affinity of benzoxazole derivatives to Aβ. Several lipophilic compounds have been reported as potential amyloid imaging probes. 2-(1-{6-[(2-Fluoroethyl)(methyl) amino]-2-naphthyl}ethylidene)malononitrile (FDDNP) was introduced as the first BBB-permeable compound for in

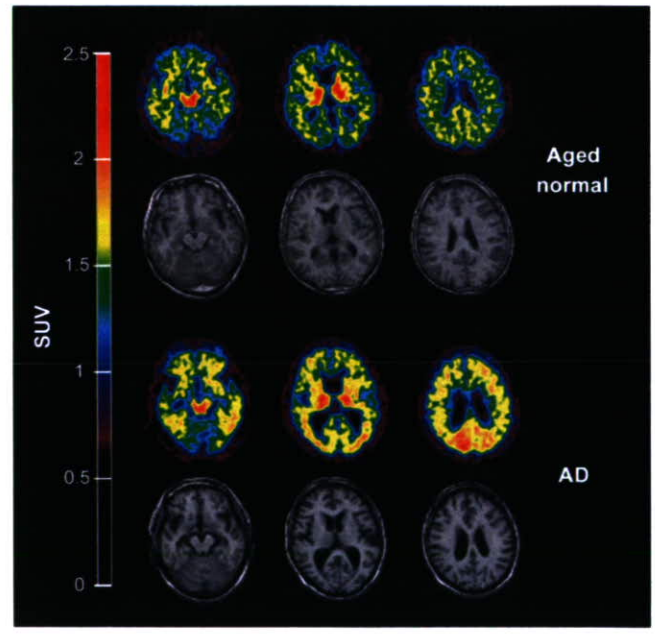

FIGURE 5. Mean SUV images between 20 and 40 min after injection of ^{11}C-BF-227 in aged normal subject (top, 70-y-old woman) and AD patient (bottom, 68-y-old woman). Coregistered MR images are shown below PET images.

TABLE 2
Regional SUV and Regional-to-Cerebellar SUV Ratio of ^{11}C-BF-227 in Normal Subjects and AD Patients

Distribution	SUV			SUV ratio			Cohen's *d*, Aged normal vs. AD
	All normal	Aged normal	AD	All normal	Aged normal	AD	
Frontal	1.13 ± 0.23	1.11 ± 0.24	1.24 ± 0.27	0.99 ± 0.04	0.99 ± 0.05	1.13 ± 0.06*	2.54
Lateral temporal	1.16 ± 0.22	1.15 ± 0.23	1.38 ± 0.30	1.03 ± 0.05	1.02 ± 0.04	1.25 ± 0.06*	4.51
Parietal	1.22 ± 0.24	1.19 ± 0.24	1.36 ± 0.30	1.08 ± 0.06	1.06 ± 0.05	1.24 ± 0.06*	3.26
Temporooccipital	1.22 ± 0.23	1.21 ± 0.24	1.35 ± 0.27	1.08 ± 0.06	1.08 ± 0.06	1.23 ± 0.09*	1.96
Occipital	1.23 ± 0.23	1.21 ± 0.24	1.32 ± 0.26	1.09 ± 0.06	1.08 ± 0.06	1.20 ± 0.07*	1.84
Anterior cingulate	1.19 ± 0.26	1.16 ± 0.26	1.27 ± 0.26	1.04 ± 0.04	1.03 ± 0.04	1.16 ± 0.06*	2.55
Posterior cingulate	1.28 ± 0.25	1.24 ± 0.25	1.38 ± 0.26	1.13 ± 0.08	1.11 ± 0.08	1.26 ± 0.04*	2.37
Medial temporal	1.33 ± 0.24	1.31 ± 0.25	1.31 ± 0.27	1.18 ± 0.07	1.17 ± 0.07	1.20 ± 0.10	0.35
Striatum	1.57 ± 0.34	1.52 ± 0.34	1.62 ± 0.34	1.38 ± 0.08	1.35 ± 0.06	1.47 ± 0.06*	2.00
Thalamus	1.78 ± 0.44	1.70 ± 0.41	1.73 ± 0.36	1.56 ± 0.12	1.51 ± 0.09	1.58 ± 0.11	0.70
Pons	1.90 ± 0.34	1.87 ± 0.34	1.91 ± 0.39	1.68 ± 0.08	1.67 ± 0.08	1.74 ± 0.09	0.82
White matter	1.64 ± 0.27	1.61 ± 0.28	1.69 ± 0.33	1.45 ± 0.11	1.44 ± 0.11	1.55 ± 0.12	0.96
Cerebellum	1.14 ± 0.23	1.13 ± 0.24	1.10 ± 0.23				

*$P < 0.05$ vs. aged normal group.

vivo imaging of amyloid. FDDNP specifically binds to both SPs and NFTs in AD brain sections (*19*). After intravenous injection of FDDNP, greater accumulation was observed in SP- and NFT-rich areas of the human brain (*20*). Thioflavin-T derivatives without any positive charge also show high permeability of the BBB. One of these compounds, PIB, was applied in a human PET study and enabled successful differentiation between AD patients and healthy normal individuals (*5*). Another amyloid-imaging agent, SB-13, was also applied in a human PET study and exhibited binding properties similar to those of PIB (*21*). Several iodinated agents, 6-iodo-2-(4′-dimethylamino-) phenyl-imidazo[1,2-*a*]-pyridine (IMPY) and I-stilbene, have also been explored for use as SPECT probes (*22*). Although validation remains necessary to determine whether retention of these agents in the neocortex truly reflects the level of amyloid deposition, such findings suggest the potential usefulness of this technique for early diagnosis of AD.

The results of the in vitro binding experiment indicate that binding of BF-227 reflects the amount of Aβ fibril deposition. In neuropathologic staining of AD brain sections, the fluorescence intensity of BF-227 is highest in the core region of mature amyloid deposits, which contain dense fibrils of Aβ. Conversely, diffuse plaques containing fewer Aβ fibrils are faintly stained by BF-227. SPs in the cerebellum are predominantly of the nonfibrillar type (*23,24*), and BF-227 only faintly stained diffuse amyloid plaques in the cerebellum. Thus, the absence of ^{11}C-BF-227 accumulation in the cerebellum of AD patients suggests the binding preference of this compound for fibrillar Aβ. This finding also indicates that the cerebellum is suitable as a reference region in the quantitative analysis of ^{11}C-BF-227 PET data.

PIB is currently the most successful of several amyloid-imaging agents. A clinical PET study in AD patients showed higher uptake of PIB in cortical areas and striatum, particularly the frontal and parietal cortices (*5–7*). In contrast, the current study demonstrated higher cortical retention of ^{11}C-BF-227 in the temporoparietal–occipital region rather than that in the frontal cortex and the striatum in AD patients. Both agents are considered to preferentially bind to the β-sheet structure of Aβ fibrils. What other factors could

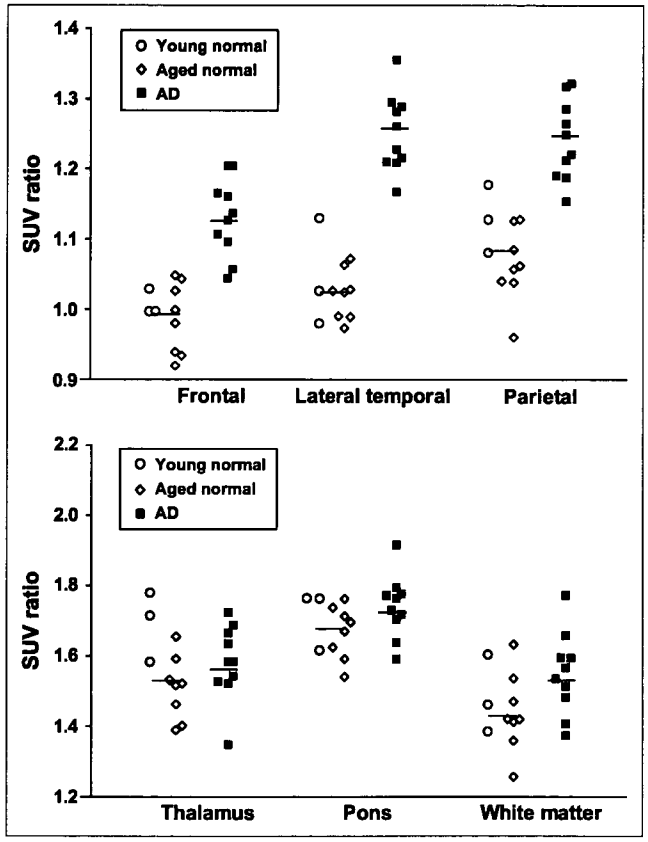

FIGURE 6. ROI/cerebellar SUV ratio in young normal subjects (○), aged normal subjects (◇), and AD patients (■). Vertical bar represents average SUV ratio in all normal subjects (n = 11) and AD patients (n = 10).

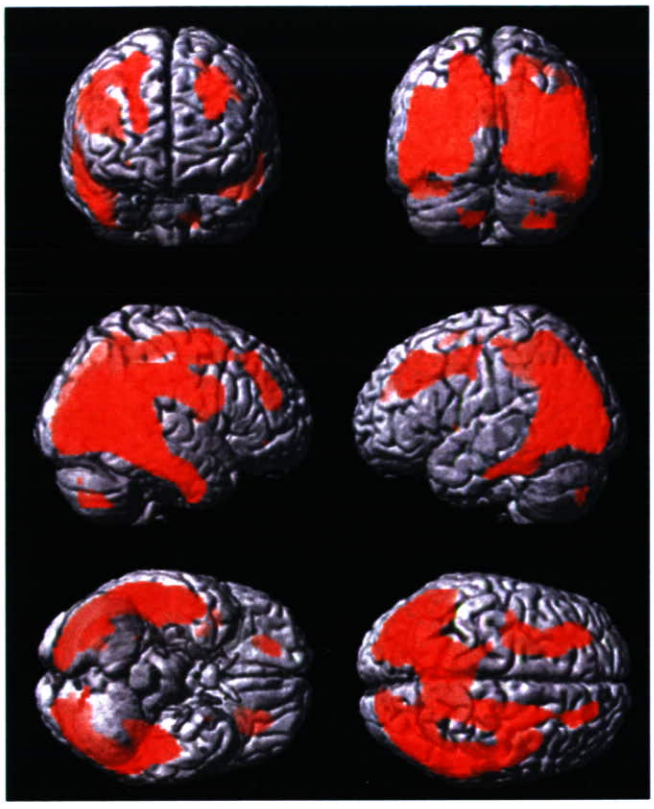

FIGURE 7. Brain regions show significantly elevated SUVs in AD patients compared with data from aged healthy subjects ($P < 0.001$, uncorrected for multiple comparisons).

have caused the difference of tracer distribution between previous PIB studies and the current BF-227 study? Generally, substantial individual variations exist in the amount and spatial distribution of amyloid deposition in AD. Thus, the discrepancy might be partially attributable to a difference in sample populations between studies. To settle this issue, a direct comparison study between PIB and BF-227 should be conducted using the same sample populations. SP is a heterogeneous class of protein aggregates with a β-pleated structure. Compact plaques consist of a dense central core of amyloid fibrils, and noncompact plaques contain less fibrillar Aβ (*25*). Therefore, it would be expected that the lower-affinity compound would tend to detect only SPs with dense Aβ fibrils and that the higher-affinity compound could bind SPs with both dense and moderately fibrillar Aβ. In AD patients, the difference between cortical and cerebellar SUV in ^{11}C-BF-227 PET was less than that in PIB PET (*5–7*), suggesting that the in vivo binding affinity of BF-227 to Aβ deposits is relatively lower than that of PIB. If so, BF-227 binds more preferentially to dense amyloid deposits than PIB. Previous neuropathologic studies have indicated that neuritic plaque densities are highest in the neocortex, especially the temporoparieto–occipital region, and lowest in the cerebellum (*18,26*). Data from SPM analysis are consistent with the postmortem distribution of neuritic plaque deposition in AD patients. Therefore, the difference in cortical distribution between BF-227 and PIB might be due to the difference in binding affinity to Aβ fibrils. A PET probe binding selectively to neuritic plaques would be less subject to Aβ pathology in the normal aging process. Thus, use of ^{11}C-BF-227 PET will allow accurate diagnosis of AD and might reduce false-positive findings in normal individuals. ^{11}C-BF-227 PET might also be useful for tracking the progression of fibrillar Aβ deposition in AD patients. Longitudinal PET investigation of AD patients will elucidate the utility of this imaging technique for monitoring disease progression in AD.

NFTs stained faintly with BF-227, suggesting that BF-227 has a relatively lower binding affinity to NFTs than SPs, which might explain the lack of significant difference in the medial temporal SUV of ^{11}C-BF-227. However, 3 AD patients (AD 1, AD 2, and AD 3 in Table 1) exhibiting high BF-227 accumulation in the cerebral cortex showed higher accumulation in the medial temporal cortex than the other AD patients. This finding might reflect the increasing deposition of amyloid plaques in the medial temporal cortex of the 3 AD patients. Thalamic and white matter accumulation of ^{11}C-BF-227 was considerable in both AD patients and normal subjects. Retention levels of ^{11}C-BF-227 in these regions were nearly identical between normal and AD groups. Therefore, these retentions are not likely to reflect AD-specific pathology. BF-227 retention in these sites may be related to the many myelinated fibers present in these structures, because myelin basic protein—one of the major myelin proteins in the brain—partially shares the same structure with amyloid fibrils, and some β-sheet binding agents bind to this protein (*27–29*). Clearance of ^{11}C-BF-227 from normal brain tissue was slower than that of PIB. This might be caused by the difference in lipophilicity between BF-227 and PIB. BF-227 ($\log P = 1.75$) is more lipophilic than PIB ($\log P = 1.20$) (*30*) because, unlike PIB, BF-227 does not have a hydroxy group. Compounds that are too lipophilic will be bound by plasma protein and undergo rapid metabolism by the liver; therefore, they may display reduced brain uptake. Moreover, lipophilic radioligands display a higher nonspecific binding in the brain and, thus, high nonspecific binding may explain the moderate difference in BF-227 uptake between AD patients and normal control subjects. In general, the introduction of a hydroxy group into a molecule changes the partition coefficient toward more hydrophilicity. Therefore, the hydroxylated BF-227 derivative would be expected to show faster clearance from normal brain tissue and a better signal-to-noise ratio than BF-227. We are now implementing the optimizing process to reduce white matter retention and plan to apply the optimized compound to the candidate for an ^{18}F-labeled PET probe.

CONCLUSION

The present study demonstrated that the benzoxazole derivative BF-227 displays high binding affinity to amyloid

plaques and high BBB permeability. The current clinical trial indicated that BF-227 has adequate safety to be used clinically as a PET probe. ^{11}C-BF-227 PET demonstrated significant retention of this agent in sites with a preference for the deposition of dense amyloid plaques and distinctly differentiated between AD patients and normal individuals. Collectively, these findings suggest that ^{11}C-BF-227 is useful for early diagnosis of AD.

ACKNOWLEDGMENTS

This study was supported by the Program for the Promotion of Fundamental Studies in Health Science by the National Institute of Biomedical Innovation, the Special Coordination Funds for Promoting Science and Technology, the Industrial Technology Research Grant Program in 2004 from the New Energy and Industrial Technology Development Organization of Japan, Health and Labour Sciences Research Grants for Translational Research from the Ministry of Health, Astrazeneca Research Grant 2004, and the Novartis Foundation for Gerontological Research. We appreciate the technical assistance of Dr. Shoichi Watanuki and Dr. Yoichi Ishikawa in the clinical PET studies and Dr. Motohisa Kato in the imaging analysis. We also thank Dr. Hiroyasu Akatsu and Dr. Takayuki Yamamoto for supplying brain samples.

REFERENCES

1. Morris JH, Nagy Z. Alzheimer's disease. In: Esiri MM, Lee VM, Trojanowski JQ, eds. *The Neuropathology of Dementia.* 2nd ed. Cambridge, U.K.: Cambridge University Press; 2004:161–206.
2. Goldman WP, Price JL, Storandt M, et al. Absence of cognitive impairment or decline in preclinical Alzheimer's disease. *Neurology.* 2001;56:361–367.
3. Price JL, Morris JC. Tangles and plaques in nondemented aging and "preclinical" Alzheimer's disease. *Ann Neurol.* 1999;45:358–368.
4. Aisen PS. The development of anti-amyloid therapy for Alzheimer's disease: from secretase modulators to polymerisation inhibitors. *CNS Drugs.* 2005;19:989–996.
5. Klunk WE, Engler H, Nordberg A, et al. Imaging brain amyloid in Alzheimer's disease with Pittsburgh Compound-B. *Ann Neurol.* 2004;55:306–319.
6. Price JC, Klunk WE, Lopresti BJ, et al. Kinetic modeling of amyloid binding in humans using PET imaging and Pittsburgh Compound-B. *J Cereb Blood Flow Metab.* 2005;25:1528–1547.
7. Lopresti BJ, Klunk WE, Mathis CA, et al. Simplified quantification of Pittsburgh Compound B amyloid imaging PET studies: a comparative analysis. *J Nucl Med.* 2005;46:1959–1972.
8. Price JL. Diagnostic criteria for Alzheimer's disease. *Neurobiol Aging.* 1997; 18(suppl):S67–S70.
9. Wang J, Dickson DW, Trojanowski JQ, Lee VM. The levels of soluble versus insoluble brain Aβ distinguish Alzheimer's disease from normal and pathologic aging. *Exp Neurol.* 1999;158:328–337.
10. Okamura N, Suemoto T, Shimadzu H, et al. Styrylbenzoxazole derivatives for in vivo imaging of amyloid plaques in the brain. *J Neurosci.* 2004;24:2535–2541.
11. Okamura N, Suemoto T, Shiomitsu T, et al. A novel imaging probe for in vivo detection of neuritic and diffuse amyloid plaques in the brain. *J Mol Neurosci.* 2004;24:247–255.
12. Shimadzu H, Suemoto T, Suzuki M, et al. Novel probes for imaging amyloid-β: F-18 and C-11 labeling of 2-(4-aminostyryl)benzoxazole derivatives. *J Labelled Compds Radiopharm.* 2004;47:181–190.
13. Jewett DM. A simple synthesis of [^{11}C]methyl triflate. *Appl Radiat Isot.* 1992;43:1383–1385.
14. Iwata R, Pascali C, Bogni A, Miyake Y, Yanai K, Ido T. A simple loop method for the automated preparation of [^{11}C]raclopride from [^{11}C]methyl triflate. *Appl Radiat Isot.* 2001;55:17–22.
15. Holcomb L, Gordon MN, McGowan E, et al. Accelerated Alzheimer-type phenotype in transgenic mice carrying both mutant amyloid precursor protein and presenilin 1 transgenes. *Nat Med.* 1998;4:97–100.
16. Friston KJ, Holmes AP, Worsley KJ, Poline JP, Frith CD, Frackowiack RSJ. Statistical parametric maps in functional imaging: a general linear approach. *Hum Brain Mapp.* 1995;2:189–210.
17. Higuchi M, Tashiro M, Arai H, et al. Glucose hypometabolism and neuropathological correlates in brains of dementia with Lewy bodies. *Exp Neurol.* 2000; 162:247–256.
18. Arnold SE, Hyman BT, Flory J, Damasio AR, Van Hoesen GW. The topographical and neuroanatomical distribution of neurofibrillary tangles and neuritic plaques in the cerebral cortex of patients with Alzheimer's disease. *Cereb Cortex.* 1991;1:103–116.
19. Agdeppa ED, Kepe V, Liu J, et al. Binding characteristics of radiofluorinated 6-dialkylamino-2-naphthylethylidene derivatives as positron emission tomography imaging probes for beta-amyloid plaques in Alzheimer's disease. *J Neurosci.* 2001;21:RC189:1–5.
20. Shoghi-Jadid K, Small GW, Agdeppa ED, et al. Localization of neurofibrillary tangles and beta-amyloid plaques in the brains of living patients with Alzheimer disease. *Am J Geriatr Psychiatry.* 2002;10:24–35.
21. Verhoeff NP, Wilson AA, Takeshita S, et al. In-vivo imaging of Alzheimer disease beta-amyloid with [^{11}C]SB-13 PET. *Am J Geriatr Psychiatry.* 2004;12: 584–595.
22. Kung HF, Kung MP, Zhuang ZP, et al. Iodinated tracers for imaging amyloid plaques in the brain. *Mol Imaging Biol.* 2003;5:418–426.
23. Yamaguchi H, Hirai S, Morimatsu M, Shoji M, Nakazato Y. Diffuse type of senile plaques in the cerebellum of Alzheimer-type dementia demonstrated by beta protein immunostain. *Acta Neuropathol (Berl).* 1989;77:314–319.
24. Yamazaki T, Yamaguchi H, Nakazato Y, Ishiguro K, Kawarabayashi T, Hirai S. Ultrastructural characterization of cerebellar diffuse plaques in Alzheimer's disease. *J Neuropathol Exp Neurol.* 1992;51:281–286.
25. Dickson DW. The pathogenesis of senile plaques. *J Neuropathol Exp Neurol.* 1997;56:321–339.
26. Joachim CL, Morris JH, Selkoe DJ. Diffuse senile plaques occur commonly in the cerebellum in Alzheimer's disease. *Am J Pathol.* 1989;135:309–319.
27. Bjelke B, Seiger A. Morphological distribution of MBP-like immunoreactivity in the brain during development. *Int J Dev Neurosci.* 1989;7:145–164.
28. Ridsdale RA, Beniac DR, Tompkins TA, Moscarello MA, Harauz G. Three-dimensional structure of myelin basic protein. II. Molecular modeling and considerations of predicted structures in multiple sclerosis. *J Biol Chem.* 1997; 272:4269–4275.
29. Stankoff B, Wang Y, Bottlaender M, et al. Imaging of CNS myelin by positron-emission tomography. *Proc Natl Acad Sci U S A.* 2006;103:9304–9309.
30. Mathis CA, Wang Y, Holt DP, Huang GF, Debnath ML, Klunk WE. Synthesis and evaluation of ^{11}C-labeled 6-substituted 2-arylbenzothiazoles as amyloid imaging agents. *J Med Chem.* 2003;46:2740–2754.

BJCP British Journal of Clinical Pharmacology

DOI:10.1111/j.1365-2125.2007.03063.x

In vivo visualization of donepezil binding in the brain of patients with Alzheimer's disease

Nobuyuki Okamura,[1] Yoshihito Funaki,[2] Manabu Tashiro,[3] Motohisa Kato,[1] Yoichi Ishikawa,[2] Masahiro Maruyama,[4] Hiroyasu Ishikawa,[5] Kenichi Meguro,[5] Ren Iwata[2] & Kazuhiko Yanai[1]

[1]Department of Pharmacology, Tohoku University Graduate School of Medicine, Sendai, [2]Division of Radiopharmaceutical Chemistry, Cyclotron and Radioisotope Center, Tohoku University, Sendai, [3]Division of Nuclear Medicine, Cyclotron and radioisotope centre, Tohoku University, Sendai, [4]Department of Geriatric and Complementary Medicine, Tohoku University Graduate School of Medicine, Sendai and [5]Department of Geriatric Behavioural Neurology, Tohoku University Graduate School of Medicine, Sendai, Japan

Correspondence
Dr Nobuyuki Okamura MD, PhD, Department of Pharmacology, Tohoku University School of Medicine, 2-1, Seiryo-machi, Aoba-ku, Sendai 980-8575, Japan.
Tel.: +81 2 2717 8058;
Fax: +81 2 2717 8060;
E-mail: oka@mail.tains.tohoku.ac.jp

Keywords
acetylcholinesterase, Alzheimer's disease, donepezil, positron emission tomography (PET)

Received
1 July 2007

Accepted
26 September 2007

Published *OnlineEarly*
7 December 2007

WHAT IS ALREADY KNOWN ABOUT THIS SUBJECT

- Deficit in central cholinergic neurotransmission is a consistent change associated with Alzheimer's disease (AD).
- Donepezil hydrochloride exhibits selective inhibition of acetylcholinesterase (AChE) and is widely used for the treatment of AD.
- The biodistribution of donepezil in the brain after administration is not precisely understood *in vivo*.
- There is no method to measure the amount of binding of orally administered donepezil to AChE.

WHAT THIS STUDY ADDS

- This study clearly visualizes the distribution of donepezil in human brain using [^{11}C]-donepezil and positron emission tomography.
- This study demonstrates prominent reduction of the donepezil binding site in the AD brain.
- This study provides methodology to measure the AChE binding occupancy of orally administered donepezil and provides a new surrogate marker for evaluation and prediction of response to donepezil treatment.

AIMS

The aims of this study were to visualize *in vivo* binding of donepezil to acetylcholinesterase (AChE) in the brain and to establish a method for measuring the amount of binding of orally administered donepezil.

METHODS

[5-^{11}C-methoxy]-donepezil ([^{11}C]-donepezil) was radiolabelled as a positron emission tomography (PET) tracer. The biodistribution of [^{11}C]-donepezil was measured by PET in 10 AD patients and six elderly normal subjects. Two AD patients underwent additional PET measurements after oral administration of donepezil for 6 months.

RESULTS

[^{11}C]-donepezil-PET images demonstrated high densities of tracer distribution in AChE-rich brain regions such as the striatum, thalamus, and cerebellum. Compared with elderly normal subjects, patients with mild AD exhibited about 18–20% reduction of donepezil binding in the neocortex and hippocampus, while patients with moderate AD exhibited about 24–30% reduction of donepezil binding throughout the brain. Orally administered donepezil (5 mg day^{-1}) induced 61.6–63.3% reduction of donepezil binding in AD brains. The distribution volume of [^{11}C]-donepezil in the hippocampus was significantly correlated with MMSE scores in AD patients.

CONCLUSIONS

[^{11}C]-donepezil-PET enables quantitative measurement of donepezil binding in the brain. AD patients exhibited reduction of donepezil binding in the brain, even in the early stage of disease. Longitudinal evaluation by this technique enables determination of AChE binding occupancy of orally administered donepezil.

Introduction

Cholinergic deficit is consistently found in the brain of patients with Alzheimer's disease (AD). Reduction in the activity of choline acetyltransferase (ChAT) and acetylcholinesterase (AChE) is evident in AD brains and correlates with cognitive decline [1, 2]. For this reason, cholinergic enhancement is a major approach to the treatment of AD. Currently, several AChE inhibitors (AChEIs) are widely prescribed to improve cognitive function in patients with AD [3]. However, not all patients respond to these treatments. It is thus important to identify factors that determine individual responses to treatment with AChEIs.

Functional imaging of cholinergic function is a useful strategy for determination of the treatment protocol of demented patients. Use of AChEIs themselves as radiotracers enables direct investigation of the pharmacokinetics of AChEIs using positron emission tomography (PET). Donepezil hydrochloride is currently the AChEI most widely used for the treatment of AD. It exhibits selective binding of AChE compared with butyrylcholinesterase (BuChE) [4]. Radiolabelled donepezil can thus be used as a tracer to measure brain concentrations of AChE. If the distribution of donepezil in the brain can be measured quantitatively by PET, this will be useful for pharmacological evaluation of AChEIs and for prediction of efficacy of treatment with donepezil. In this study, we performed PET examinations using [5-^{11}C-methoxy]-donepezil ([^{11}C]-donepezil) and determined the *in vivo* binding characteristics of donepezil in AD patients.

Methods

Subjects and patients

Six elderly normal subjects and 10 patients with probable AD were studied to examine the distribution of [^{11}C]-donepezil in the brain. The AD patients were recruited through The Tohoku University Hospital Dementia Patients Registry. The diagnosis of AD was made according to the National Institute of Neurologic Disorders and Stroke/Alzheimer's Disease and Related Disorders Association (NINCDS-ADRDA) criteria. AD patients were further divided into two groups by severity: a mild AD group ($n = 5$; MMSE score ≥ 23 points) and a moderate AD group ($n = 5$; MMSE score < 20 points). The normal control group was comprised of volunteers without impairment of cognitive function who had no cerebrovascular lesions on magnetic resonance (MR) images. After complete description of the study to the patients and subjects, written informed consent was obtained from them. PET study was performed within 3 months after the completion of a medical and neuropsychological examination. Although no significant difference in age was observed between the mild AD group and elderly normal group, the moderate AD group was older than the elderly normal group (Table 1). The MMSE score of the elderly normal subjects (mean ± SD 29.7 ± 0.8) was significantly higher than that of the mild AD (25.0 ± 1.6) and moderate AD (15.4 ± 2.7) subjects.

Table 1

Subjects and patients demographics

		Gender	Age	MMSE
Elderly normal	AN1	M	64	30
	AN2	M	61	30
	AN3	F	59	30
	AN4	F	60	30
	AN5	M	74	28
	AN6	F	75	30
	Mean		65.5	29.7
	SD		7.2	0.8
Mild AD	AD1	F	77	24
	AD2	F	72	23
	AD3	M	71	26
	AD4	F	66	25
	AD5	M	69	27
	Mean		71.0	25.0
	SD		4.1	1.6
Moderate AD	AD6	F	77	14
	AD7	F	78	12
	AD8	F	79	19
	AD9	M	84	17
	AD10	F	81	15
	Mean		79.8	15.4
	SD		2.8	2.7

Radiosynthesis of [5-^{11}C-methoxy]-donepezil

Synthesis of [^{11}C]-donepezil was performed (Figure 1) as described previously [5]. Briefly, 5'-O-desmethylprecursor (M2) was dissolved in methylethylketone and then tetrabutylammonium hydroxide was added. [^{11}C]-Methyl iodide was prepared from [^{11}C]-CO_2 and converted to [^{11}C]-methyl triflate ([^{11}C]-MeOTf). [^{11}C]-Donepezil was produced on the loop from [^{11}C]-MeOTf and purified by high performance liquid chromatography (HPLC). The radioactivity obtained was 155.4–814 MBq (4.2–22 mCi), and the radiochemical yield was 25–30% based on [^{11}C]-MeOTf after decay-correction. Specific activity was 111–354 GBq μmol^{-1} at the end of synthesis (30–40 min from the end of ^{11}C production). Radiochemical purity was greater than 99%.

PET acquisition protocols

The protocol of the PET study was approved by the Committee on Clinical Investigation at The Tohoku University School of Medicine and the Advisory Committee on Radioactive Substances at Tohoku University. The [^{11}C]-donepezil PET study was performed using a SET-2400 W PET scanner (Shimadzu Inc., Japan) under resting condition with eyes closed. Following a ^{68}Ge/Ga transmission scan of 7 min duration, an emission scan was started soon after intravenous injection of 7.1–9.5 mCi of [^{11}C]-donepezil. Emission

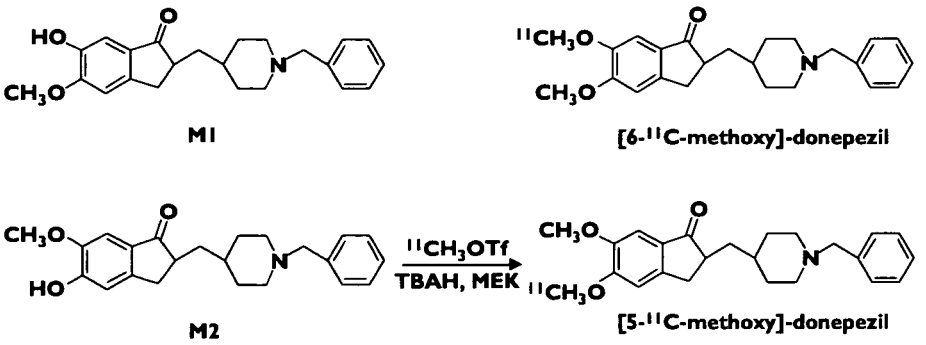

Figure 1
Chemical structures and radiosynthesis of donepezil and its metabolites

data were acquired for 60 min. Standardized uptake value (SUV) images were obtained by normalizing tissue concentration by injected dose and body mass. Arterialized venous blood samples were obtained from a hand vein, heated in a far-infrared mat, and radioactivity was measured in a well-type scintillation counter. Sampled plasma (2 ml) was denaturated with 1 M $HClO_4$: MeCN (7 : 3) and centrifuged at 3000 × *g* for 3 min. The supernatant solution was injected into a column (YMC ODS A-324, YMC Co., Ltd, Kyoto, Japan; 10 mm i.d. × 30 cm long) with a solvent system of 0.1 M ammonium formate : acetonitrile (60 : 40) at a flow rate of 5.0 ml min^{-1}. The eluates were collected at time intervals of 0.5 min and were counted for radioactivity with a gamma counter.

Image analysis

Region of interest (ROI) analysis was performed to evaluate the regional distribution of [^{11}C]-donepezil. Circular ROIs (1.0 cm in diameter) were placed on individual axial PET images in the cerebellar hemisphere, striatum, thalamus, lateral frontal cortex (Brodmann's areas (BA) 44, 45, 46, and 47), lateral temporal cortex (BA 20, 21, and 22), parietal cortex (BA 39 and 40), occipital cortex (BA 17), anterior cingulate cortex (BA 24 and 32), posterior cingulate cortex (BA 23 and 31), and medial temporal cortex (BA 27, 28, 34, and 35), referring to the individual MR images. To measure donepezil -binding AChE density in the brain, the distribution volume (DV), the ratio of [^{11}C]-donepezil concentration in tissue to that in plasma at equilibrium, was calculated by Logan's graphical analysis [6], since donepezil reversibly binds to AChE. Using this method, the DV in each ROI was determined from the slopes obtained from the values of each ROI and input function from metabolite-corrected plasma radioactivity. The slopes were determined from the last 15 points of the respective regions. Details of the quantitative analysis will be described elsewhere.

Statistical analysis

Differences in age, MMSE score, and DV among the three groups were evaluated by one-way analysis of variance (ANOVA) followed by Bonferroni's multiple comparison test (GraphPad Prism Software). For each analysis, findings were considered significant at $P < 0.05$.

Results

Tissue time activity curves (TAC) of [^{11}C]-donepezil in the brain indicated initial rapid uptake of radioactivity followed by gradual clearance from the brain in both elderly normal (Figure 2A) and AD subjects (Figure 2B). Relatively high concentrations of radioactivity of [^{11}C]-donepezil were observed in AChE-rich brain regions such as the striatum, thalamus, and cerebellum, whereas radioactivity uptake in the neocortex including frontal, temporal, and parietal cortices was moderate. Plasma radioactivity of [^{11}C]-donepezil peaked at 30–60 s postinjection, followed by a rapid decline (Figure 2C). Proportions of unchanged [^{11}C]-donepezil in plasma were 91.0 ± 7.0%, 88.1 ± 12.5%, and 82.5 ± 5.1% at 5, 15, and 30 min postinjection, respectively. The metabolite-corrected plasma time–activity curve was used to calculate specific DVs from the region-of-interest-derived regional time–activity curve. [^{11}C]-donepezil exhibited linear regression curves on Logan plot analysis in all brain regions examined (Figure 3). Since the slopes of the regression lines represent the DV of the tracer, these findings indicate a higher DV of donepezil in the striatum than in the frontal cortex. Parametric images of [^{11}C]-donepezil DV clearly revealed higher concentrations of tracer distribution in the striatum and cerebellum than in the neocortex. Patients with mild AD exhibited reduction of DV in the hippocampus and neocortex, compared with elderly normal subjects. The magnitude of DV reduction in the mild AD group was about 20% in the hippocampus and 18% in temporal and parietal cortices. In patients with moderate AD, DV reduction was evident throughout the brain (Figure 4, Figure 5, Table 2). The magnitude of DV reduction was about 30% in the hippocampus and 24% in frontal, temporal, and parietal cortices. Two AD patients (AD3 and AD10) underwent another PET scan after treatment with 5 mg donepezil for 6 months. Orally

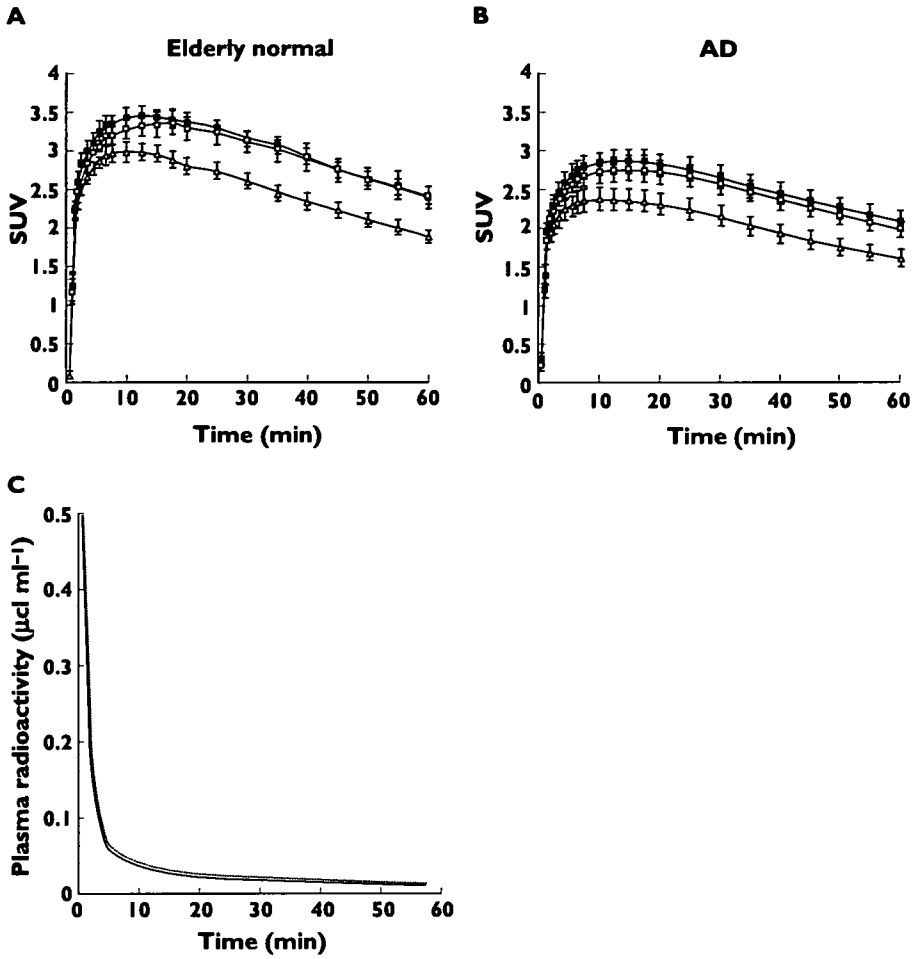

Figure 2

Time activity data for [^{11}C]-donepezil PET in humans. Brain SUV time activity curves for elderly normal subjects (A) and AD patients (B), and plasma time activity curve (C) are shown. The dotted line indicates total time activity curve and the solid line indicates metabolite-corrected time activity curve

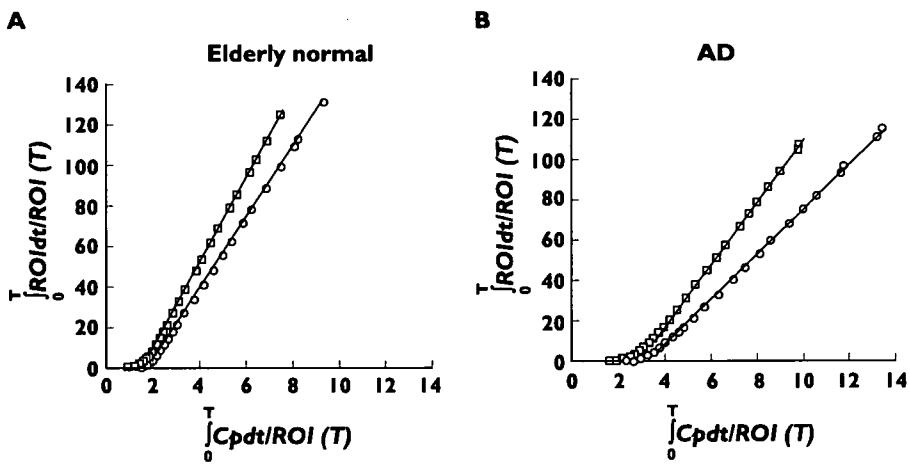

Figure 3

Logan plots for the striatum (□) and frontal cortex (○) for elderly normal subjects (A) and AD patients (B). *Cp*: plasma concentration of tracer, ROI: region of interest, *T*: time after injection

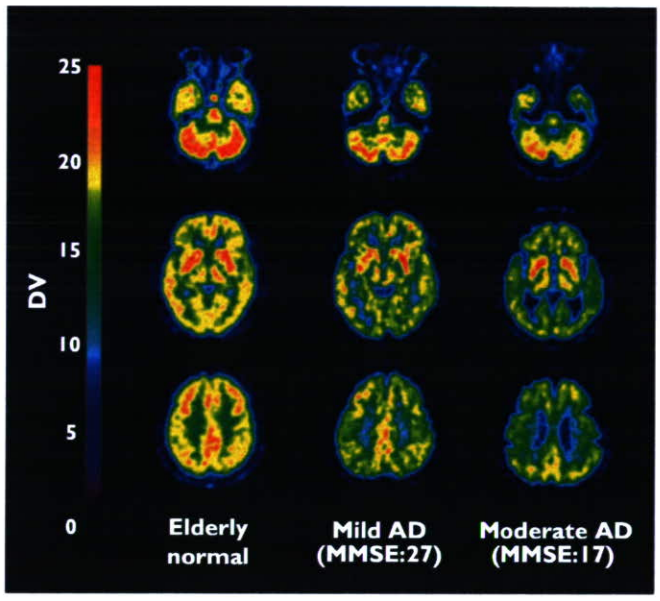

Figure 4

Distribution volume images of [^{11}C]-donepezil in elderly normal subjects (left), patients with mild AD (middle), and patients with moderate AD (right)

administered donepezil induced substantial reduction of DV in all regions of brain examined (Figure 6). Mean DV reduction in patient 1 (AD3) was 61.6% (55.5% in the cerebellum, 65.2% in the striatum, 63.6% in the thalamus, 62.5% in the frontal cortex, 61.6% in the temporal cortex, 59.6% in the parietal cortex, 62.6% in the occipital cortex, 60.3% in the anterior cingulate cortex, 59.5% in the posterior cingulate cortex and 65.5% in the medial temporal cortex). Mean DV reduction in patient 2 (AD10) was 63.3% (59.9% in the cerebellum, 72.0% in the striatum, 60.6% in the thalamus, 61.6% in the frontal cortex, 62.9% in the temporal cortex, 62.4% in the parietal cortex, 54.2% in the occipital cortex, 62.4% in the anterior cingulate cortex, 57.9% in the posterior cingulate cortex and 78.8% in medial temporal cortex). Finally, the correlation of donepezil binding with severity of dementia was examined within the AD patient group. As shown in Figure 7, the DV value in the hippocampus was significantly correlated with MMSE scores of AD patients.

Discussion

Currently, *in vivo* monitoring of brain AChE activity using positron emission tomography (PET) is beneficial in developing strategies for dementia therapy. [^{11}C]-MP4A and [^{11}C]-PMP, which are metabolically trapped acetylcholine analogues, have been successfully applied to the evaluation of AChE activity in the brain [7, 8]. PET studies in AD patients have demonstrated reduction of AChE activity in the early stage of disease, with the degree of reduction correlating with cognitive dysfunction [9, 10]. Another strategy involves use of AChEIs themselves as radiotracers. This method enables direct investigation of the pharmacokinetics of AChEIs. [^{11}C]-physostigmine [11], [^{11}C]-methyltacrine [12], and [^{11}C]-CP-126 998 [13] have been designed as radiotracers for clinical PET study. *In vivo* imaging techniques using such radiotracers can measure the concentrations of tracer-binding AChE. If these radiotracers and therapeutic drugs competitively bind to AChE, the occupancy of binding sites on AChE by therapeutic drugs could be measured by subtraction of post-treatment from pretreatment PET scans.

This PET study demonstrated that intravenously administered [^{11}C]-donepezil rapidly enters the brain and is mainly distributed in the striatum, thalamus, and cerebellum, which are known to contain high densities of AChE compared with the cerebral cortex and hippocampus. This finding is consistent with the findings of our previous study in rats [5]. The regional distribution of [^{11}C]-donepezil was also consistent with regional AChE activity determined in a human postmortem study [14], suggesting selective binding of donepezil to AChE.

Post-treatment evaluation following administration of 5 mg donepezil day^{-1} revealed a remarkable reduction (61.6–63.3% compared with pretreatment scan) of [^{11}C]-donepezil binding throughout the brain. This indicates that the AChE occupancy by donepezil, when administered in daily doses of 5 mg, was about 35–40% in these two patients. A previous PET study using [^{11}C]-MP4A revealed a mean 39% reduction in AChE activity after oral administration of 3–5 mg donepezil [15]. Intravenous administration of donepezil in monkeys also resulted in a mean 27% reduction of AChE activity at a dose of 100 μg kg^{-1} [16]. These findings together suggest that inhibition of AChE activity matches occupancy of AChEI binding sites. Moreover, orally administered donepezil (5 mg) induced substantial inhibition (43–62%) of the binding of another radiotracer, [^{11}C]-CP-126 998, to AChE [13]. This finding is roughly consistent with our observations. The amount of binding of orally administered donepezil to AChE is considered a key factor in determining therapeutic response. AChE binding occupancy by orally administered donepezil could be modulated by blood–brain barrier permeability, tissue distribution, metabolism, and also by AChE density in the brain. *In vivo* evaluation of AChE occupancy could thus be a powerful strategy for determining the optimal dose of donepezil. In the future, quantitative evaluation of donepezil binding sites might be used to optimize regimens of treatment with donepezil and to predict the response to treatment. To this purpose, red blood cell AChE inhibition has been explored as a peripheral surrogate marker for the activity of AChEIs [17]. In a future study, we plan to examine the relationship between red blood cell AChE inhibition and [^{11}C]-donepezil binding in the brain.

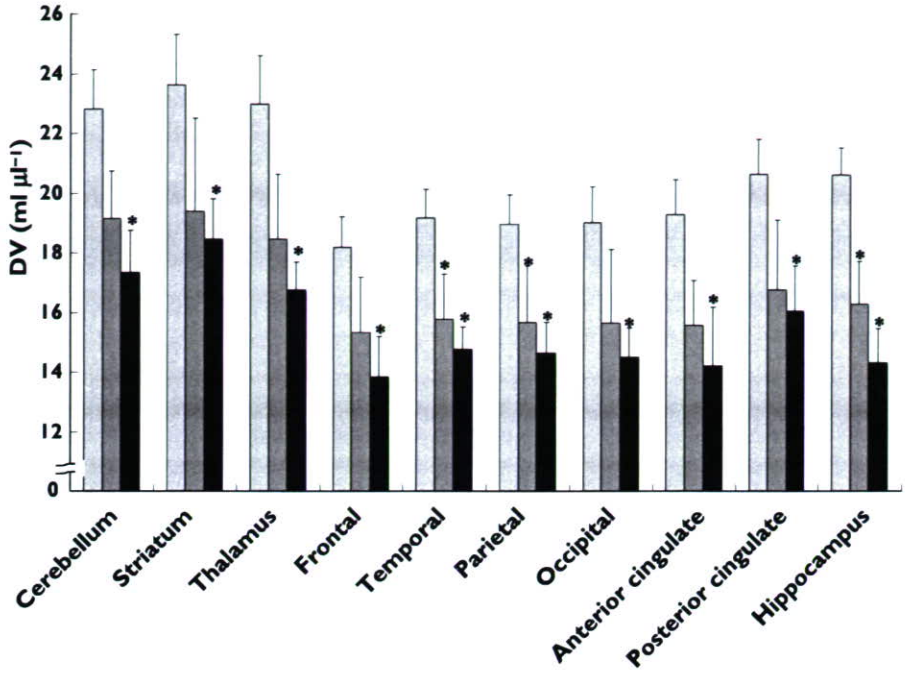

Figure 5

Regional distribution volume data in elderly normal subjects (□), mild AD (▨), and moderate AD patients (■)

Table 2

Regional distribution volume of [^{11}C]-donepezil in elderly normal subjects and AD patients (mean ± SEM)

	Elderly normal	Mild AD	Moderate AD
Cerebellum	23.4 ± 3.5	19.6 ± 1.4	17.6 ± 1.4*
Striatum	24.0 ± 4.1	20.0 ± 3.1	18.5 ± 1.6*
Thalamus	23.4 ± 4.1	19.0 ± 2.1	17.1 ± 1.0*
Frontal	18.5 ± 2.5	15.8 ± 1.8	14.0 ± 1.5*
Temporal	19.7 ± 2.6	16.2 ± 1.3*	15.1 ± 0.9*
Parietal	19.5 ± 2.7	16.1 ± 1.7*	15.0 ± 1.1*
Occipital	19.4 ± 3.2	16.1 ± 2.3	14.6 ± 1.1*
Anterior cingulate	19.6 ± 2.6	16.2 ± 1.7	14.7 ± 1.9*
Posterior cingulate	21.1 ± 3.0	17.2 ± 2.3	16.3 ± 1.7*
Hippocampus	21.4 ± 2.1	17.3 ± 2.1*	14.8 ± 1.2*

*P < 0.05, significantly different from aged normal group.

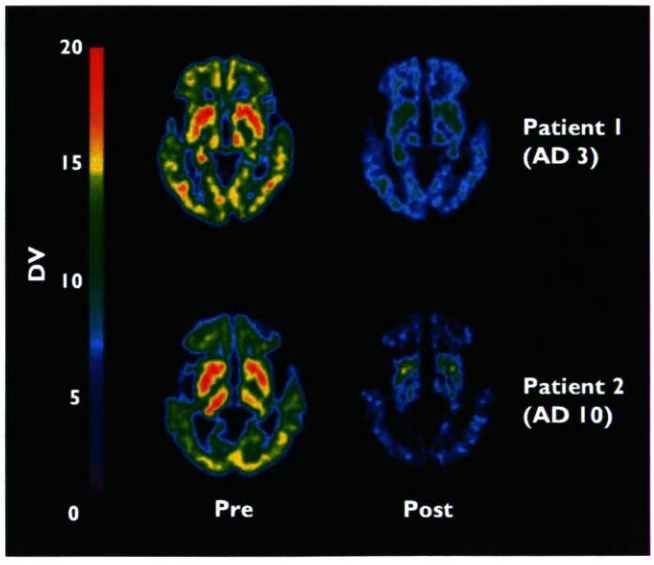

Figure 6

Distribution volume images before and after oral administration of donepezil in AD patients

Patients with moderate AD exhibited significant reduction of [^{11}C]-donepezil DV in all brain regions examined, in comparison with elderly normal subjects. Furthermore, temporo-parietal and hippocampal DVs were significantly reduced even in patients with mild AD, compared with elderly normal group. These reductions suggest early involvement of the cholinergic system in AD, since the AChE in brain is predominantly located in presynaptic cholinergic neurones [18]. A previous [^{11}C]-MP4A PET study demonstrated 21% reduction of hippocampal AChE activity in patients with early onset AD [19]. We observed an approximately 20% reduction in hippocampal DV in the mild AD group and 30% reduction in the moderate AD group. These findings suggest that the concentration of donepezil-binding AChE is matched by regional AChE activity. In a postmortem study, AD patients exhibited reduction of AChE activity, and this reduction was correlated with the severity of dementia [20, 21]. We observed

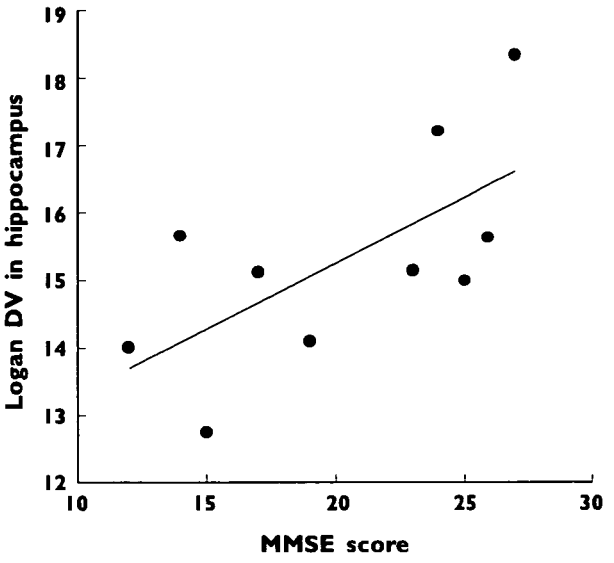

Figure 7

Correlation between MMSE scores and distribution volume in the hippocampus of AD patients. Pearson $r = 0.659$ and $p = 0.038$

that DV in the hippocampus was correlated with the cognitive status in AD patients, a finding in accord with postmortem data. However, it is important to note that the partial volume effect due to structural atrophy might cause the underestimation of DV in the hippocampus. Analysis after partial volume correction is therefore needed to establish further the relationship between the regional DV of [^{11}C]-donepezil and the severity of dementia in AD.

Compared with previously reported findings of PET imaging with [^{11}C]-MP4A [9] and [^{11}C]-PMP [10], the present [^{11}C]-donepezil-PET study demonstrated a relatively higher cortical retention of radiotracer, suggesting the existence of alternative binding sites for donepezil other than AChE. Donepezil is reported to have high binding affinity for σ_1-receptors, which are widely distributed in the brain including the cerebral cortex, hippocampus, and cerebellum [22–24]. A recent human PET study using a σ_1-receptor-specific radioligand demonstrated prominent reduction of σ_1-receptor density in the cerebral cortex and cerebellum of AD patients [25]. Thus, concomitant binding of donepezil to σ_1-receptors might have contributed to the distinctive distribution of [^{11}C]-donepezil we observed in the brain.

Previously, the tracer kinetics of [^{11}C]-donepezil with labelling of the methoxy group at position 6 ([6-^{11}C-methoxy]-donepezil) were examined in mice and rabbits, to test this agent as a candidate for a PET radioligand [26]. However, the regional brain distribution of this radiotracer did not reflect the distribution of AChE in the brain. In contrast, our previous study yielded successful *in vivo* visualization of AChE by donepezil labelled with ^{11}C at the methoxy group at position 5 ([5-^{11}C-methoxy]-donepezil) [5]. The differences between these findings might be attributable to the affinity of unlabelled metabolites to AChE. Indeed, the unlabelled metabolite of [6-^{11}C-methoxy]-donepezil (M1 in Figure 1) has high binding affinity for AChE ($IC_{50} = 6.4$ nM), resulting in competition for binding between ^{11}C-labelled tracer and unlabelled metabolite, while the metabolite of [5-^{11}C-methoxy]-donepezil (M2 in Figure 1) exhibits lower affinity of binding to AChE ($IC_{50} = 1.1$ μM) than M1. [5-^{11}C-methoxy]-donepezil is thus suitable for detection of AChE *in vivo*. In addition, the specific radioactivity of [5-^{11}C-methoxy]-donepezil in this study (111–354 GBq μmol^{-1}) was higher than that of [6-^{11}C-methoxy]-donepezil in a previous study [26]. High specific activity of [^{11}C]-donepezil might therefore be another contributing factor of successful visualization of AChE.

In this study, the distribution of donepezil in human brain was successfully visualized using [^{11}C]-donepezil and PET. Graphical analysis by Logan plots can be used to obtain quantitative estimates of specific donepezil binding. AD patients exhibited significant reduction of donepezil distribution, even in the early stages of disease. This imaging technique will be useful as a new surrogate marker for evaluation of treatment with donepezil.

This work was in part supported by Grants-in-Aid for scientific research (No. 17390156 for K.Yanai and 18019004 for N. Okamura) from the Japan Society of Promotion of Science (JSPS) and the Ministry of Education, Culture, Sports, Science and Technology in Japan, as well as by a grant from the Japan Society of Technology (JST) on research and education in 'molecular imaging'. The authors thank the volunteers, Dr Syoichi Watanuki for PET operation and Mrs Kazuko Takeda for taking care of the volunteers.

REFERENCES

1 Davies P, Maloney AJ. Selective loss of central cholinergic neurons in Alzheimer's disease. Lancet 1976; 2: 1403.

2 Coyle JT, Price DL, DeLong MR. Alzheimer's disease: a disorder of cortical cholinergic innervation. Science 1983; 219: 1184–90.

3 Giacobini E. Cholinesterase inhibitors: from the Calabar bean to Alzheimer therapy. In: Cholinesterases and Cholinesterase Inhibitors, ed. Giacobini E. London: 2000.

4 Sugimoto H, Ogura H, Arai Y, Iimura Y, Yamanishi Y. Research and development of donepezil hydrochloride, a new type of acetylcholinesterase inhibitor. Jpn J Pharmacol 2002; 89: 7–20.

5 Funaki Y, Kato M, Iwata R, Sakurai E, Sakurai E, Tashiro M, Ido T, Yanai K. Evaluation of the binding characteristics of [5-(11) C-methoxy]-donepezil in the rat brain for *in vivo* visualization of acetylcholinesterase. J Pharmacol Sci 2003; 91: 105–12.

6 Logan J. Graphical analysis of PET data applied to reversible and irreversible tracers. Nucl Med Biol 2000; 27: 661–70.

7 Kilbourn MR, Snyder SE, Sherman PS, Kuhl DE. *In vivo* studies of acetylcholinesterase activity using a labeled substrate, N-[^{11}C]methylpiperdin-4-yl propionate ([^{11}C]PMP). Synapse 1996; 22: 123–31.

8 Irie T, Fukushi K, Namba H, Iyo M, Tamagami H, Nagatsuka S, Ikota N. Brain acetylcholinesterase activity: validation of a PET tracer in a rat model of Alzheimer's disease. J Nucl Med 1996; 37: 649–55.

9 Iyo M, Namba H, Fukushi K, Shinotoh H, Nagatsuka S, Suhara T, Sudo Y, Suzuki K, Irie T. Measurement of acetylcholinesterase by positron emission tomography in the brains of healthy controls and patients with Alzheimer's disease. Lancet 1997; 349: 1805–9.

10 Kuhl DE, Koeppe RA, Minoshima S, Snyder SE, Ficaro EP, Foster NL, Frey KA, Kilbourn MR. *In vivo* mapping of cerebral acetylcholinesterase activity in aging and Alzheimer's disease. Neurology 1999; 52: 691–9.

11 Blomqvist G, Tavitian B, Pappata S, Crouzel C, Jobert A, Doignon I, Di Giamberardino L. Quantitative measurement of cerebral acetylcholinesterase using [^{11}C]physostigmine and positron emission tomography. J Cereb Blood Flow Metab 2001; 21: 114–31.

12 Tavitian B, Pappata S, Bonnot-Lours S, Prenant C, Jobert A, Crouzel C, Di Giamberardino L. Positron emission tomography study of [^{11}C]methyl-tetrahydroaminoacridine (methyl-tacrine) in baboon brain. Eur J Pharmacol 1993; 236: 229–38.

13 Bencherif B, Endres CJ, Musachio JL, Villalobos A, Hilton J, Scheffel U, Dannals RF, Williams S, Frost JJ. PET imaging of brain acetylcholinesterase using [^{11}C]CP-126 998, a brain selective enzyme inhibitor. Synapse 2002; 45: 1–9.

14 Finkelstein Y, Wolff M, Biegon A. Brain acetylcholinesterase after acute parathion poisoning: a comparative quantitative histochemical analysis post mortem. Ann Neurol 1988; 24: 252–7.

15 Shinotoh H, Aotsuka A, Fukushi K, Nagatsuka S, Tanaka N, Ota T, Tanada S, Irie T. Effect of donepezil on brain acetylcholinesterase activity in patients with AD measured by PET. Neurology 2001; 56: 408–10.

16 Shiraishi T, Kikuchi T, Fukushi K, Shinotoh H, Nagatsuka S, Tanaka N, Ota T, Sato K, Hirano S, Tanada S, Iyo M, Irie T. Estimation of plasma IC_{50} of donepezil hydrochloride for brain acetylcholinesterase inhibition in monkey using N-[^{11}C]methylpiperidin-4-yl acetate ([^{11}C]MP4A) and PET. Neuropsychopharmacology 2005; 30: 2154–61.

17 Sramek JJ, Cutler NR. RBC cholinesterase inhibition: a useful surrogate marker for cholinesterase inhibitor activity in Alzheimer disease therapy? Alzheimer Dis Assoc Disord 2000; 14: 216–27.

18 Mesulam MM, Geula C. Overlap between acetylcholinesterase-rich and choline acetyltransferase-positive (cholinergic) axons in human cerebral cortex. Brain Res 1992; 577: 112–20.

19 Shinotoh H, Namba H, Fukushi K, Nagatsuka S, Tanaka N, Aotsuka A, Ota T, Tanada S, Irie T. Progressive loss of cortical acetylcholinesterase activity in association with cognitive decline in Alzheimer's disease: a positron emission tomography study. Ann Neurol 2000; 48: 194–200.

20 Zubenko GS, Moossy J, Martinez AJ, Rao GR, Kopp U, Hanin I. A brain regional analysis of morphologic and cholinergic abnormalities in Alzheimer's disease. Arch Neurol 1989; 46: 634–8.

21 Prohovnik I, Perl DP, Davis KL, Libow L, Lesser G, Haroutunian V. Dissociation of neuropathology from severity of dementia in late-onset Alzheimer disease. Neurology 2006; 66: 49–55.

22 Kato K, Hayako H, Ishihara Y, Marui S, Iwane M, Miyamoto M. TAK-147, an acetylcholinesterase inhibitor, increases choline acetyltransferase activity in cultured rat septal cholinergic neurons. Neurosci Lett 1999; 260: 5–8.

23 Guitart X, Codony X, Monroy X. Sigma receptors: biology and therapeutic potential. Psychopharmacology 2004; 174: 301–19.

24 Sakata M, Kimura Y, Naganawa M, Oda K, Ishii K, Chihara K, Ishiwata K. Mapping of human cerebral sigma1 receptors using positron emission tomography and [^{11}C]SA4503. Neuroimage 2007; 35: 1–8.

25 Hashimoto K, Ishiwata K. Sigma receptor ligands: possible application as therapeutic drugs and as radiopharmaceuticals. Curr Pharm Des 2006; 12: 3857–76.

26 De Vos F, Santens P, Vermeirsch H, Dewolf I, Dumont F, Slegers G, Dierckx RA, De Reuck J. Pharmacological evaluation of [^{11}C]donepezil as a tracer for visualization of acetylcholinesterase by PET. Nucl Med Biol 2000; 27: 745–7.

Geriatr Gerontol Int 2007; 7: 393–400

ORIGINAL ARTICLE: BIOLOGY

Binding and safety profile of novel benzoxazole derivative for *in vivo* imaging of amyloid deposits in Alzheimer's disease

Nobuyuki Okamura,[1] Shozo Furumoto,[2] Yoshihito Funaki,[3] Takahiro Suemoto,[4] Motohisa Kato,[1] Yoichi Ishikawa,[3] Satoshi Ito,[1] Hiroyasu Akatsu,[5] Takayuki Yamamoto,[5] Tohru Sawada,[4] Hiroyuki Arai,[6] Yukitsuka Kudo[2] and Kazuhiko Yanai[1]

[1]Department of Pharmacology, Tohoku University Graduate School of Medicine, [2]Tohoku University Biomedical Engineering Research Organization (TUBERO), [3]Division of Radiopharmaceutical Chemistry, Cyclotron and Radioisotope Center, Tohoku University, [6]Center for Asian Traditional Medicine, Department of Geriatrics and Gerontology, Tohoku University School of Medicine, Sendai, [4]BF Research Institute, Osaka, and [5]Fukushimura Hospital, Toyohashi, Japan

Background: *In vivo* detection of amyloid deposits in the brain is potentially useful for early diagnosis of Alzheimer's disease (AD) and tracking the efficacy of anti-amyloid therapy.

Methods: To develop an amyloid-binding agent for positron emission tomography, we screened over 2600 compounds.

Results: We found benzoxazole derivatives as candidate compounds for *in vivo* amyloid imaging probes. One of these agents, 2-(2-[2-dimethylaminothiazol-5-yl]ethenyl)-6-(2-[fluoro]ethoxy)benzoxazole (BF-227), displays high binding affinity to Aβ fibrils. BF-227 binding increased linearly with increasing Aβ fibril formation. In temporal and hippocampal AD brain sections, BF-227 selectively bound to amyloid plaques. In contrast, no staining was evident in the cerebellum. Compared with the previously reported compound BF-168, ^{18}F-labeled BF-227 displayed selective *in vivo* labeling of amyloid fibrils and rapid washout from white matter areas in an Aβ-injected rat model. An acute and subacute toxicity study of BF-227 indicated sufficient safety for clinical use as a positron emission tomography probe.

Conclusions: These findings suggest that BF-227 is feasible as an *in vivo* imaging probe of amyloid deposits in AD patients.

Keywords: Alzheimer's disease, amyloid, positron emission tomography, senile plaques.

Introduction

Progressive deposition of senile plaques (SP) and neurofibrillary tangles (NFT) is a critical event in the pathogenesis of Alzheimer's disease (AD). These lesions precede the presentation of clinical symptoms of dementia.[1] For early or presymptomatic diagnosis of AD, non-invasive detection of these lesions using positron emission tomography (PET) is a potentially

Accepted for publication 22 August 2007.

Correspondence: Dr Nobuyuki Okamura MD PhD, Department of Pharmacology, Tohoku University Graduate School of Medicine, 2-1 Seiryo-machi, Aoba-ku, Sendai 980-8575, Japan. Email: oka@mail.tains.tohoku.ac.jp

doi: 10.1111/j.1447-0594.2007.00430.x

useful technique.[2] To achieve successful *in vivo* imaging using PET, sensitive and selective contrast agents to these lesions are needed. Congo red and thioflavin T have represented attractive lead compounds as developing amyloid-imaging agents, because these compounds selectively bind to β-pleated sheet structures and are commonly used for histochemical staining of SP. However, the permeability of these compounds through the blood–brain barrier (BBB) is extremely limited.[3] The chemical structure must thus be optimized to provide appropriate lipophilicity without changing the binding properties to amyloid. Thioflavin T derivatives without any positive charge show high permeability of the BBB. One of these compounds, 6OH-BTA-1 (PIB), has been applied in a human PET study and enabled successful detection of early AD patients.[4] Another compound, 2-(1-[6-{<2-fluoroethyl><methyl>amino}-2-naphthyl]ethylidene) malononitrile (FDDNP), is extremely lipophilic and can easily penetrate the BBB, and specifically binds to both SP and NFT in AD brain sections.[5] After i.v. injection of FDDNP, greater accumulation was observed in SP- and NFT-rich areas of the human brain.[6] Although validation is still required as to whether retention of these agents in the neocortex truly reflects levels of amyloid deposition, such findings suggest the potential usefulness of this technique for early diagnosis of AD.

We have previously demonstrated a novel series of compounds including 6-(2-fluoroethoxy)-2-(2-[4-methylaminophenyl]ethenyl)benzoxazole (BF-168) and (2-[4-methylaminophenyl]ethenyl)-5-fluorobenzoxazole (BF-145) as promising candidates for *in vivo* imaging probes of SP.[7–9] These benzoxazole derivatives demonstrate high binding affinity for Aβ aggregates and high BBB permeability, suggesting potential utility as *in vivo* amyloid-binding agents. However, for the application of these compounds to clinical PET studies, the pharmacokinetic properties and pharmacological safety of these molecules requires improvement. This study describes the characterization of an optimized benzoxazole derivative, 2-(2-[2-dimethylaminothiazol-5-yl]ethenyl)-6-(2-[fluoro]ethoxy) benzoxazole (BF-227), as a candidate *in vivo* amyloid-imaging agent in humans.

Methods

Preparation of the compounds

BF-168, BF-227 (Fig. 1) and the precursor compounds for ^{18}F-labeled agents were custom-synthesized by Tanabe R & D Service (Osaka, Japan). Synthesis of (^{18}F)BF-168 was performed by reacting 2-(4-methylaminophenyl)-6-(2-tosyloxyethoxy) benzoxazole (Tanabe R & D Service) with (^{18}F)KF and Kryptofix 222 (Merck, Darmstadt, Germany) in acetonitrile at 80°C for 20 min, as described previously.[8] Radiosynthesis of (^{18}F)BF-227 was performed using the same method. After subsequent high-performance liquid chromatography (HPLC) purification, ^{18}F-labeled compounds were obtained (Fig. 1). Details of the radiosynthetic methods will be described elsewhere.

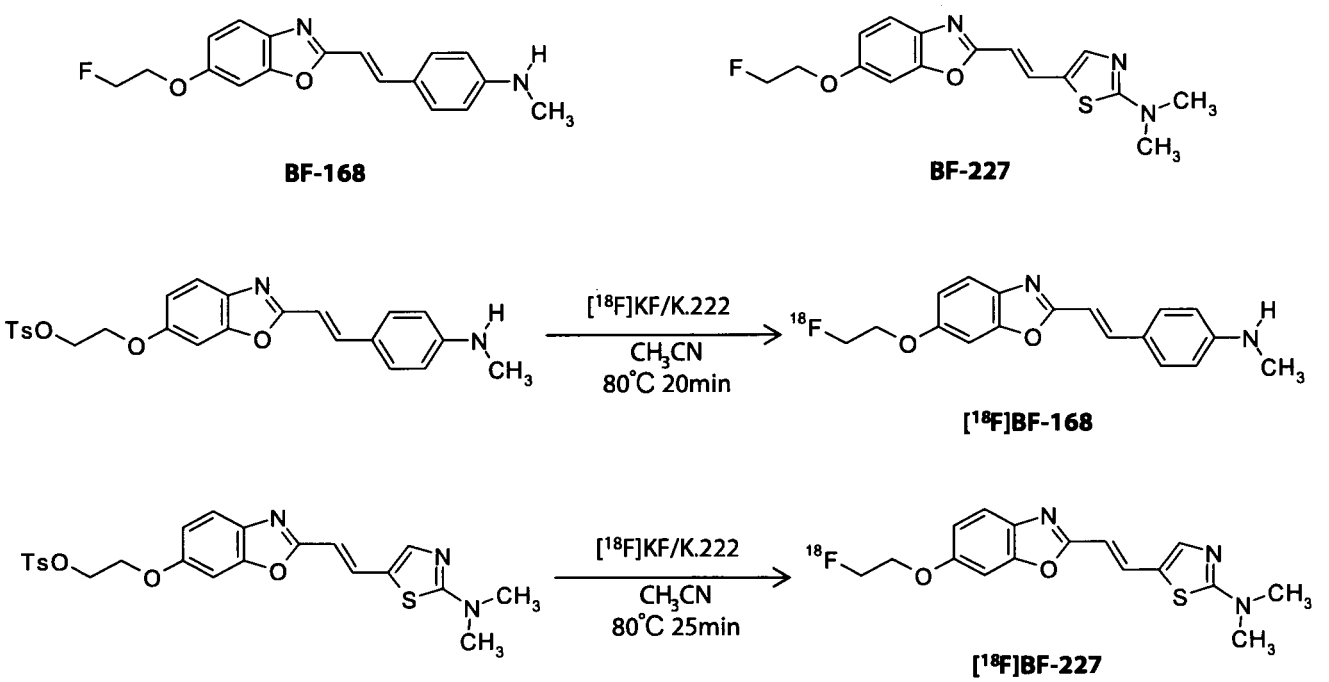

Figure 1 Chemical structures and radiosynthesis of BF-168 and BF-227.

In vitro *binding assays*

Binding affinities of the compounds for synthetic Aβ aggregates were examined as described previously.[7] Briefly, solid-form Aβ1–40 (Peptide Institute, Osaka, Japan) was dissolved in 10 mmol/L potassium phosphate buffer (pH 7.4) and incubated at 37°C for 72 h. The binding assay was performed by mixing aggregated Aβ1–40 with the appropriate concentration of ^{18}F-labeled BF-227, unlabeled BF-227 and dimethyl sulfoxide. After incubation for 10 min at room temperature, the binding mixture was filtered using a cell harvester (Model M-24; Brandel, Gaithersburg, MD, USA) and filters containing bound ^{18}F ligand were counted using a γ-counter. The dissociation constant (K_d) of BF-227 was determined by Scatchard analysis.

Fluorometric analysis of BF-227 binding with Aβ fibrils was performed using the following method. A total of 20 μmol/L of Aβ1–40 or Aβ1–42 (Peptide Institute) in 50 mmol/L of potassium phosphate buffer (pH 7.4) was incubated at 37°C on a Vibrax VXR shaker (IKA, Cincinnati, OH, USA) at 0.56 *g*. Before fluorometric analysis, Aβ solutions were sonicated for 3 min at 45 kHz using a VS-100III ultrasonic cleaner (Iuchi, Osaka, Japan). In fluorometry, Aβ1–40 and Aβ1–42 solutions at 0, 4, 8 and 24 h after the start of incubation were mixed with the same volume of BF-227 solution (5 μmol/L final concentration). After determination of the optimal excitation wavelength for the mixture of BF-227 and Aβ, fluorescence spectra were measured using a Gemini XS microplate spectrofluorometer (Molecular Devices, Sunnyvale, CA, USA). In addition, fluorescence spectra for the mixture of 5 μM BF-227 and different concentrations of Aβ1–40 or Aβ1–42 (0.15, 0.5 1.5, 2.5, 5 and 10 μmol/L final concentrations) at 96 h after incubation (fibrillar Aβ) were measured using the microplate spectrofluorometer. The same measurements were also performed using Aβ1–40 and Aβ1–42 with no incubation (non-fibrillar Aβ). All measurements were performed in triplicate.

Neuropathological staining

Postmortem brain tissues from an autopsy-confirmed AD case (69-year-old man) were obtained from Fukushimura Hospital (Toyohashi, Japan). Experiments were performed under the regulations of the Ethics Committee of BF Research Institute. Serial sections (6-μm thick) from paraffin-embedded blocks of temporal cortex and cerebellum were prepared in xylene and ethanol. Before staining, quenching of autofluorescence was performed as described previously. Quenched tissue sections were immersed in 100 μmol/L of BF-227 solution for 10 min or 0.01% 1-bromo-2,5-bis(3-carboxy-4-hydroxystyryl)benzene (BSB) solution containing 50% ethanol for 30 min. Sections stained with BF-227 were then dipped briefly into water and rinsed in phosphate-buffered saline (PBS) for 60 min before coverslipping with Fluor Save Reagent (Calbiochem, La Jolla, CA, USA), and examined using an Eclipse E800 microscope (Nikon, Tokyo, Japan) equipped with a V-2A filter set (excitation 380–420 nm, dichroic mirror 430 nm, longpass filter 450 nm). Sections stained with BSB were dipped briefly in tap water and then in 50% ethanol, then washed in PBS for 60 min before coverslipping, followed by fluorescent microscopy using a BV-2A filter set (excitation 400–440 nm, dichroic mirror 455 nm, longpass filter 470 nm). In addition, adjacent sections were immunostained using monoclonal antibody (mAb) against Aβ (6F/3D; Dako A/S, Glostrup, Denmark). After pretreatment with 90% formic acid for 5 min, sections were immersed in blocking solution for 30 min and then incubated for 60 min at 37°C with 6F/3D at a dilution of 1:50. Following incubation, sections were processed by the avidin–biotin method using a Pathostain ABC-POD(M) Kit (Wako, Osaka, Japan) and diaminobenzidine tetrahydrochloride. Fluorescence intensity of three different brain slices stained with BF-227 was analyzed by defining regions of interest (ROI) and measuring the intensity of fluorescence within gray and white matter using Lumina Vision software (Mitani, Fukui, Japan). Ratios of gray matter ROI to white matter ROI were calculated as an indicator of stainability and statistical comparisons were performed using ANOVA and Scheffe post-hoc tests.

Labeling of amyloid deposits in Aβ-injected rat model

Aβ1–40 (Peptide Institute) was dissolved at 500 μmol/L in 50 mmol/L potassium phosphate buffer and incubated at 37°C for 4 days. An Aβ-injected rat model was created as described previously.[10] Briefly, Wistar rats (male, 200–250 g, SLC, Shizuoka, Japan) were injected with Aβ peptides unilaterally and potassium phosphate buffer contralaterally into each amygdala using a stereotaxic instrument (Model 5000, David Kopf, Tujunga, CA, USA). Injection coordinates measured from the bregma and skull surface (anteroposterior, −3.0 mm; mediolateral, ±5.0 mm; dorsoventral, −8.8 mm) were determined based on a stereotaxic atlas.[11] A volume of 1.0 μL was administered over 2 min using a microsyringe and glass cannula (tip diameter, 170–250 μm). At 3 days after injection of Aβ and vehicle, (^{18}F)BF-168 (72.8 MBq) or (^{18}F)BF-227 (58.9 MBq) were administered into the femoral vein of anesthetized rats. Rats were killed by decapitation at 180 min postinjection and the brains were removed and frozen. An OTF cryostat (Bright Instruments, Huntingdon, UK) was used to cut 30-μm thick frozen sections, which were then dried and exposed to a BAS-III imaging plate for 18 h. Autoradiographic images were obtained using a BAS2000 scanner system

(Fuji Film, Tokyo, Japan). After autoradiographic examination, the same sections were stained with thioflavin-S to confirm the presence of amyloid plaques.

Toxicity study in mice

A non-GLP (good laboratory practice) toxicity study was performed using female and male ICR mice (weight, 22–32 g). The Ethics Committee of BF Research Institute approved the protocol for these experiments. Animals were kept in a temperature-controlled environment (21.2–23.5°C) with a 12-h light–dark cycle and ad libitum access to food and water. In the acute toxicity study, animals were divided into one control group and three treated groups, with 10 animals (five males, five females) in each group. The control group received injection of vehicle alone, while each treated group received i.v. injection of BF-227 solution in doses of 0.1, 1 or 10 mg/kg. Animals were observed for 8 days after administration to identify any changes in general behavior or bodyweight. In the subacute toxicity study, animals were divided into one control group and two treated groups (2.5 and 25 μg/kg), with 10 animals (five females, five males) in each group. The control group received injection of vehicle alone and each treated group received i.v. injection of BF-227 solution for 14 days (once daily). Animals were weighed at 3, 7, 9 and 14 days after administration. At the end of the experiment, animals were sacrificed and examined at autopsy. Selected organs (brain, heart, liver, lung and kidney) were removed, weighed and examined microscopically by a pathologist.

Results

Binding characteristics of BF-227 for Aβ fibrils

In vitro binding assay indicated that BF-227 shows high binding affinity for Aβ fibrils. K_d for Aβ1–40 fibrils was 1.0 ± 1.4 nmol/L, comparable to previously reported levels for amyloid imaging agents[12] (Fig. 2). Binding ability of BF-227 to Aβ was also examined by fluorometric analysis, as BF-227 is highly fluorescent. In the mixture of BF-227 and Aβ peptides, fluorescence intensity of BF-227 increased as Aβ1–40 (Fig. 3a) and Aβ1–42 (data not shown) incubation time advanced. BF-227 fluorescence also increased in a linear manner with increasing concentrations of fibrillar Aβ1–42 (Fig. 3b) or Aβ1–40 (data not shown), but did not increase in mixture with non-fibrillar Aβ. These results suggest that degree of BF-227 binding reflects the amount of Aβ fibril formation.

Neuropathological staining in AD brain sections

Neuropathological examination using BF-227 indicated that amyloid plaques were clearly stained with BF-227 in AD brain sections (Fig. 4a). In particular, cored plaques stained brightly with this compound. This staining pattern correlated well with Aβ immunostaining in adjacent sections (Fig. 4b). BF-227 staining was further compared to staining using BSB, a Congo red derivative. In contrast to clear staining of SP and NFT with BSB (Fig. 4c), BF-227 primarily stained SP, with faint staining of NFT. Preferential binding of BF-227 to SP rather than NFT represents a similar characteristic to the previously reported compound BF-145. BF-227 staining was subsequently performed in three different regions (temporal lobe, hippocampus and cerebellum) of an AD brain. In temporal (Fig. 5a) and hippocampal (Fig. 5b) sections, cored plaques stained brightly with BF-227. In contrast, no staining was evident in the cerebellum (Fig. 5c). Fluorometric measurement of these brain sections indicated that overall level of stainability in the cerebellum differed significantly from that in the temporal cortex and hippocampus (Fig. 5d), suggesting the binding specificity of this compound to AD pathology.

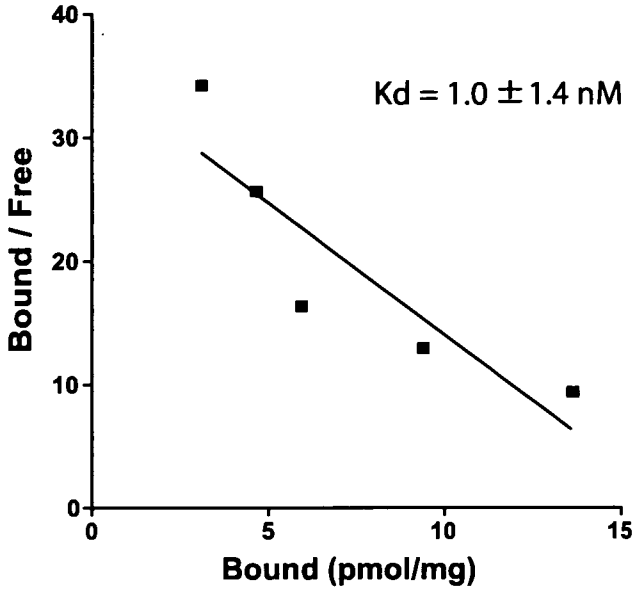

Figure 2 Scatchard plots of (^{18}F)BF-227 binding to synthetic Aβ fibrils.

Intravenous administration of ^{18}F-labeled agents in Aβ-injected rat model

In vivo binding ability of (^{18}F)BF-168 and (^{18}F)BF-227 to Aβ fibrils was further evaluated by the autoradiographic experiment in the Aβ-injected rat model. In an image of the brain section at 180 min postinjection of ^{18}F-labeled agents (Fig. 6), Aβ aggregates were clearly labeled with both agents, suggesting the usefulness of these agents as *in vivo* amyloid-imaging probes. However, non-specific

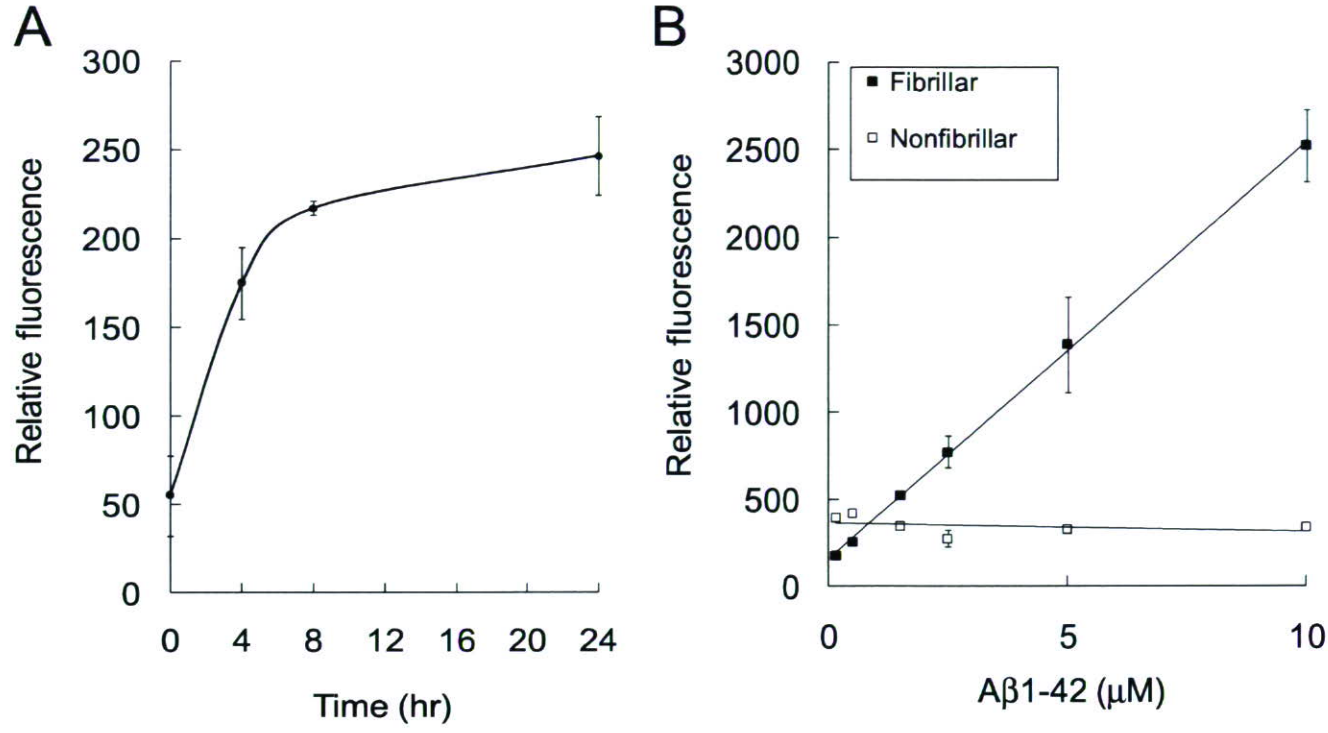

Figure 3 *In vitro* binding of BF-227 with Aβ peptides. Fluorescence intensity of BF-227 increased with Aβ incubation time (A). BF-227 fluorescence also increased linearly with concentrations of fibrillar Aβ, but did not increase in mixture with non-fibrillar Aβ (B).

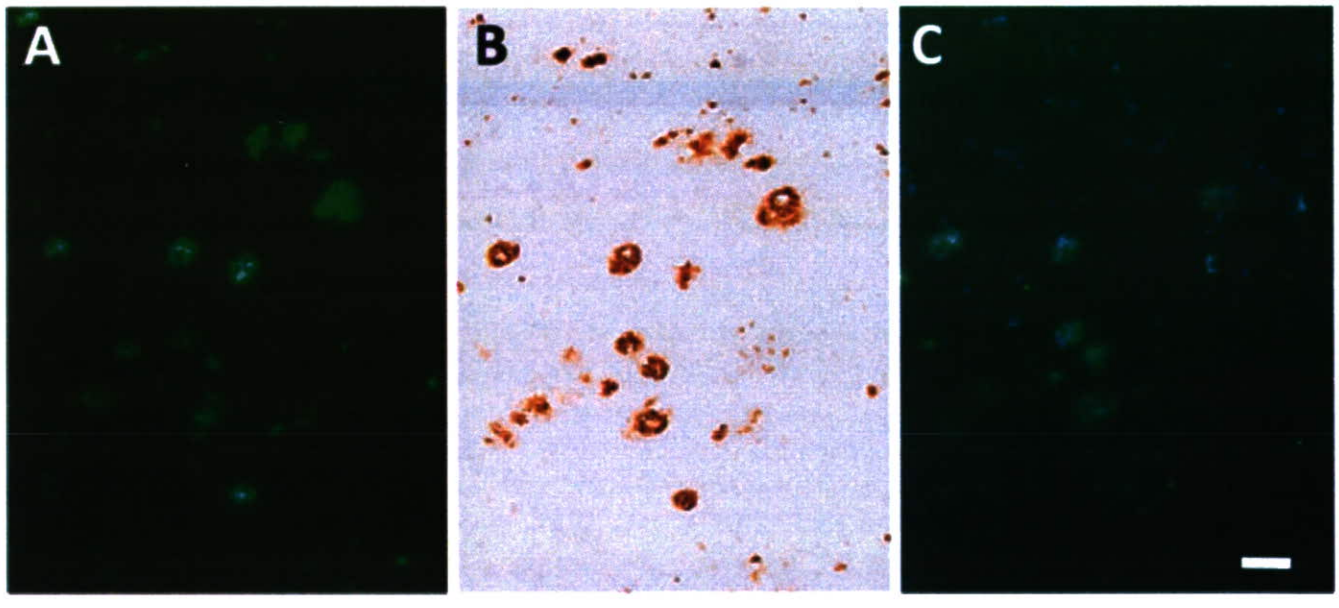

Figure 4 Neuropathological staining of Alzheimer's disease (AD) temporal brain sections by BF-227. Senile plaques are clearly stained with BF-227 (A). This staining correlates well with Aβ immunostaining in adjacent sections (B). BSB stains both senile plaques and neurofibrillary tangles (C). Bar, 200 μm.

retention of (^{18}F)BF-227 in the white matter was much less than that of (^{18}F)BF-168. This resulted in better hot spot-to-background contrast for (^{18}F)BF-227 (Fig. 6b) compared to (^{18}F)BF-168 (Fig. 6a).

Toxicity study of BF-227

In the acute toxicity study, i.v. administration of BF-227 in doses 0.1–10 mg/kg did not produce any significant